No. 349
July 2004

High Speed Model Testing With Drag Reduction

Department of Naval Architecture and
Marine Engineering

High Speed Model Testing With Drag Reduction

S. F. Zalek, R. F. Beck, S. L. Ceccio (University of Michigan)
A. M. Reed (David Taylor Model Basin, Carderock Division, Naval Surface Warfare Center)

July 2004

Department of Naval Architecture
and Marine Engineering

University of Michigan

Acknowledgement

The Office of Naval Research funded this research under contract number N00014-02-1-0389. The technical representative was Patrick Purtell. The National Defense Science and Engineering Graduate (NDSEG) fellowship program also supported this research by providing the graduate student fellowship funding for Steve Zalek, the principle author.

Contents

List of Figures

List of Tables

Executive Summary

Many important military and civilian proposed projects are beyond the state of the art in our understanding of the characteristics of high Reynolds number flows. The proposed 70 knot Army fast logistics ship, 250 knot underwater missiles, and civilian very high-speed ferries are examples of high-speed vehicles that can not be accurately model tested because of our lack of knowledge concerning the proper scaling laws for extremely high Reynolds number flows. The hydrodynamic (and wind) forces on such a ship operating at full speed will be enormous, and the flow patterns will be very complex. The friction drag is expected to be the largest contributor to the total drag. The obvious course of action is to focus significant effort on reducing the friction drag as much as possible using some type of active or passive friction drag reducing (FDR) technology.

Understanding the fundamental physics of the FDR technology is prudent, prior to making an attempt to implement the FDR technology onto a full-scale, operational vessel, if there is to be a chance of success within a reasonable period of time. Several attempts to "shotgun" a solution from promising, but basic, laboratory results to deployment of a prototype system onto a full-scale ship have met with disappointment. Numerical and experimental analysis of turbulent flows at the smallest observable scales has yielded significantly new insight into the mechanisms of turbulence, and the behavior of the major structures within the boundary layer. The "streak-liftup-hairpin-burst-sweep" cycle of turbulence regeneration provides a conceptual model around which we may build a strategy to affect the control of turbulence. One or more of these events within the cycle of turbulence regeneration must be controlled in order to reduce total friction drag. The interaction between each of these mechanisms has only recently been observed and conceptualized through advanced numerical and experimental means, and the model may undergo further refinement as the investigation continues. Additional investigation into the mechanisms of turbulence is critical to finding the FDR technology that would most appropriately match the needs of a high-speed ocean-going vessel.

It would be neither practical nor appropriate to investigate all of the possible existing FDR technologies for application to the high-speed ship. Preliminary engineering estimates indicate that the fast logistics ship total drag must be reduced by a factor of two (Genalis, 2000). Friction drag represents the greatest percentage of total drag, estimated to be approximately 70 percent of total drag. Assuming the residual 30 percent of total drag (form, wave, spray, etc.) already represents the optimum, and cannot be reduced, the friction drag must be reduced by a factor of four. This limits the FDR technologies that will be investigated to those that have demonstrated a reasonable chance of reducing friction drag by a factor of four, or by approximately 75 percent. The FDR technologies that come close to meeting this criterion are: microbubbles, polymers, surfactants, ventilation with super repellent coating, microfibers with polymer, and high viscosity fluid. Synergistic combinations of these technologies may yield even more significant friction drag reduction.

The FDR technology must not only reduce friction drag significantly, but also be capable of practical implementation on a full-scale ship, and be reliable under at-sea conditions, possibly including severe storms, and high speed maneuvering. FDR technologies that are "passive", or "always on" such as ventilation by super-cavitation would be the most preferable. Technologies where the drag reduction could be initiated with limited auxiliary equipment and a readily available (and low mass) "feed stock", such as microbubbles or blower induced ventilation, would be the next-most preferable technology. Technologies that require exotic auxiliary equipment and/or a significant quantity of "feed stock" to be carried by the ship, such as polymers or surfactants, would be the least preferable. This criterion effectively eliminates the fiber-polymer technology, due to practical considerations, and may ultimately eliminate polymers, surfactants and high viscosity fluid.

The experiments that are required to study the fundamental fluid mechanic problems associated with the design of high-speed ships and submarines are very involved and will require special instrumentation and testing facilities. It is most likely that a single facility will not suffice for all the tests.

Initial testing of a FDR technology will be very "basic" (testing at high speed on a flat, cavitation-free plate in fresh water), focusing on understanding the fundamental physics of the technology, and the mechanisms of turbulence. Subsequent tests on complex shapes, including various pressure gradients, will be necessary to determine how the FDR technology will behave in complex flows (evaluating the effect of persistence, etc.).

No test facility currently exists that meets all of the requirements to investigate the mechanisms of turbulence or test the FDR technologies at the necessary fluid speeds, pressure gradients, and length scales. To construct a new facility dedicated to this purpose may be prohibitively expensive in both time and capital. A few of the existing facilities come close to meeting some of the testing requirements, and could be modified into acceptable test facilities, even if not perfect, if some engineering improvements were made. The discussion in this paper will show that the LCC facility and the Detroit River Dam site represent the kind of facility that is appropriate for the

initial phase of the testing. A separate program has already been initiated to begin making several small improvements to the LCC to support the first phase of FDR testing. A phased-approach to making the engineering improvements to the LCC, in conjunction with the FDR testing process, makes the best use of time and capital. Minor improvements to the LCC system for little capital will allow initial FDR testing to begin with capabilities far beyond what has previously been documented. The results of these initial tests may help point the direction of subsequent testing, possibly in ways that were previously unforeseen. Subsequent engineering improvements can be developed while FDR testing continues. Therefore, the most efficient and prudent solution is to make the best use of the LCC test facility, making incremental improvements as FDR testing evolves.

The full battery of FDR tests will require high speed, submerged non-cavitating and cavitating flow tests; high speed free surface tests; and full-scale open water tests. In keeping with the prudent but efficient approach toward testing, the Carderock High Speed Carriage #6 should be considered the facility of choice for the free surface tests, after the appropriate engineering improvements are made. However, making improvements to Carriage #6 should wait until satisfactory progress has been made during the initial stages of testing at the LCC to warrant the capital expenditure.

The final phase of testing will be on a full-scale, high-speed, open water test platform. The FDR will have to prove its effectiveness in seawater, in a complex flow with a dynamic, complex pressure gradient, subject to a hull with imperfections from construction and marine fouling. Some of these effects may be simulated individually in the high-speed channel or towing tank, but there is no substitute for evaluating the combined effect on FDR performance. The test platform will also be the field laboratory for developing a robust and effective FDR delivery system. Having a reliable, maintainable, and cost effective delivery system is just as important as having an effective FDR technology itself.

1 INTRODUCTION

Many important military and civilian proposed projects are beyond the state of the art in our understanding of the characteristics of high Reynolds number flows. The proposed 70 knot Army fast logistics ship, 250 knot underwater missiles, and civilian very high-speed ferries are examples of high-speed vehicles that can not be accurately model tested because of our lack of knowledge concerning the proper scaling laws for extremely high Reynolds number flows. To gain such knowledge will require fundamental investigations into high Reynolds number hydrodynamics. Both experimental tests and analytic/numerical investigations are needed. In the end, designers prefer analysis over experiments because experiments are both expensive and time consuming. However, development of analytic/numerical techniques requires detailed experiments for insight and validation. In addition, at least until the analytic/numerical methods are sufficiently accurate, naval architects will continue to require experiments that can be scaled to full size in order to validate design predictions.

For example, the proposed fast logistics ship is currently beyond the capabilities of any existing vessel, due to the combination of its size and speed requirements. The hydrodynamic (and wind) forces on such a ship operating at full speed will be enormous, and the flow patterns will be very complex. Ship types that have been considered for this mission are: semi-lifting displacement hull form; multi-hull catamaran, or trimaran hull; hydrofoil; and surface effect ship (SES). Each ship type has advantages and disadvantages. Broadbent and Kennell (2001) analyzed fifty different existing high-speed ship forms and configurations, and extrapolated these ship performance characteristics out to match the desired performance of the fast logistics ship. From this analysis it becomes obvious that significant technological improvement will be required in the areas of ship structural design, engine room configuration, propulsion power density and efficiency, and ship drag reduction in order to meet an even modest set of high-speed operational characteristics. The Broadbent and Kennell (2001) analysis leans toward a semi-lifting trimaran displacement hull with transom stern. The DARPA study by Dimotakis, *et al.*, (2000) concluded that a hydrofoil hull form was advantageous. Estimates for total drag and its component makeup are gross, at best. Dimotakis, *et al.*, (2000) estimates that the hydrofoil fast logistics ship would experience 70 percent friction drag, 22 percent induced drag, 6 percent wave drag, and 2 percent spray drag. A high-speed displacement hull's drag components may distribute as 70 percent friction drag, 3 percent form drag, 25 percent wave drag and 2 percent spray drag. The ship hull type and trade-offs between mission requirements and hydrodynamic optimization will determine the magnitude and balance of the drag components. In any case, the friction drag is expected to be the largest contributor to the total drag. In order for the fast logistics ship to meet its mission objectives, it is expected that the total ship drag must be reduced by a factor of two. Given that friction drag is the largest component of total drag, the obvious course of action is to focus significant effort on reducing the friction drag as much as possible using some type of active or passive friction drag reducing technology. Today, reduction in friction drag is usually accomplished with reduction in the wetted area of the hull and the application of hydrodynamic fairing. Further reductions of friction drag have been demonstrated in the laboratory, but these (sometimes exotic) methods have not generally been applied to ocean-going vessels.

Development and implementation of drag reduction technology will require testing on both the laboratory and prototype scale. Any proposed method will have to be evaluated in the harsh flow conditions present near the hull of a high-speed vessel transiting the open ocean. Friction drag reduction (FDR) processes observed in small laboratory scale experiments may not readily relate to those found on large-scale ships. If a viable drag reduction method is found, naval architects must learn how to predict its influence on the performance of full-scale ships, and this would likely involve a combination of model-scale tests with analytical/numerical predictions. Again, testing of drag reduction methods using small, towed models will not yield scaleable results. Moreover, analytical and numerical scaling tools must be validated by a detailed experimental database. Consequently, advancement of FDR technology will require experimental facilities that can be used for both fundamental experiments and scale-model evaluation.

In ship hydrodynamics applications, high Reynolds numbers, $\boldsymbol{R}$, may be achieved by long vessels (Aircraft Carrier USS *Nimitz* (CVN-68), L = 1,040 ft, V = 38 knots, Re = 5.2×10^9), high speeds (L = 200 ft, V = 100 knots, Re = 2.6×10^9), or a combination of both. One of the difficulties of predicting the behavior of such high Reynolds number flows is that most experiments are conducted in laboratory-scale facilities where the Reynolds number is typically two or more orders of magnitude smaller. To relate the results of the experiments to full scale, scaling laws are required that can only be developed if a complete understanding of the flow physics is available. The flow physics can only be determined by a detailed set of experiments at both high and low Reynolds numbers.

For example, a study of turbulent drag reduction (for ocean going vessel application) by additives such as polymers or microbubbles at high Reynolds numbers on a flat plate would require the detailed experimental measurements of the following quantities:

- Base flow (*i.e.* without drag reduction agent injection): Average skin friction, static pressure, dynamic surface pressures, local shear stresses, average flow velocity profiles and turbulence measurements in the near-wall region.
- Base flow with polymer injection: The physical properties such as molecular weight, viscosity, etc. of the fluid/polymer will have to be characterized. The same measurements described for the base flow are needed here as well. In addition, the polymer concentration and conformation in the near-wall flow should be measured.
- Base flow with microbubble injection: The measurements described for the base flow are again needed. In addition, the characteristics of the bubbly flow such as void fraction and bubble size distributions in the near wall region

While this list represents the ideal type of measurements to be conducted to gather enough understanding of the physics of the flows under consideration, issues related to dimensions and resolution will need to be further assessed. The Karman number, which represents the ratio of the largest eddy scales (of the order of the boundary layer thickness) to the smallest eddy scale (on the order of one wall unit) could be, depending on final length and speed considerations, larger than 10^6. Consequently, the physical dimensions of the flow need to be large for the near wall region to be properly resolved. It should also be noted that most of the measurement techniques listed have never been attempted at high speeds and large scales. Some of the techniques will not be readily applicable for very high Re, which might require modifications or consideration of completely new ones.

The study will be incomplete in its assessment of practical implementation if issues such as surface roughness and fouling effects as well as the saltwater environment are not addressed as well. Surface roughness is an important consideration in all high Reynolds number experiments, but it becomes even more important when the processes of interest take place in the logarithmic region of the boundary layer. Even if polymer/microbubble drag reduction technologies are proven effective in the laboratory, problems such as flow-induced polymer scission or others might well limit the scope for practical implementation in a saltwater environment over a rough surface. The effects of pressure gradients and the free surface require careful consideration as well. Little work has been conducted on the natural bubble generation by ship flows. How the latter can affect microbubble drag reduction will need to be addressed. The possibility of using different drag reducing agents (*i.e.* fibers, surfactants, etc.) or combinations could be studied as well.

In this report, we will discuss the new knowledge that will be required, the experiments that must be made to gain that knowledge, and the experimental facilities that will be required to develop and evaluate friction drag reduction technologies for high-speed, ocean-going vessels. We will briefly review how drag on ships is characterized and currently predicted (Sections 2 and 3) and minimized (Section 4). Our understanding of flow in a high Reynolds number turbulent boundary layer is reviewed (Section 5). Current and proposed methods of reducing skin friction are reviewed in (Section 6), and the challenge of their application to ships is discussed (Section 7). We discuss what types of experimental facilities must be available in order to develop, evaluate, and scale friction drag reduction technologies for application to ships (Section 8). Lastly, we will conclude this report with some recommendations going forward (Section 9).

2 COMPONENTS OF SURFACE SHIP DRAG

The total drag on a ship can be sub divided into *wave drag*, *viscous drag*, and *secondary drag*. This division is traditional and somewhat arbitrary, and there are loss-making mechanisms that may not be logically included in a particular category (*e.g.* induced drag created by submerged lifting surfaces may be incorporated into the "viscous drag" term, or included into the "secondary drag" term). However, these three categories represent the largest percentages of ship drag.

Wave Drag: Only vessels operating on or near the free surface (near enough to generate waves) experience wave drag. Wave drag is the drag a vessel would experience even if it operated in an inviscid fluid due to displacement of the free-surface, and is equivalent to the energy carried away by the Kelvin wave system in the far field. The wave drag can be determined by taking a "wave cut" and computing the energy in the wave system. This energy can then be related to the resistance of the vessel that generated the wave system. In theory, any wave cut can be used. However, in practice a longitudinal cut taken along the path of travel or a transverse cut behind the ship is usually

used. In addition, the cut is normally taken far enough from the ship so that the local waves have decayed and only the far field waves remain. A longitudinal wave cut is convenient for model tests because it is easy to fix the wave probe and run the model by it. Experimentally, transverse cuts are problematic because of the interference of the viscous wake behind the vessel. For inviscid computations, the transverse wave cut might be the easiest to use. In both experiments and computations, care must be taken that the wave heights accurately represent the wave system. In experiments, this means wall reflection and viscous decay must be properly taken into account. For computations, reflections from the computational boundaries and numerical dissipation can cause difficulties.

Viscous Drag: Viscous drag is due to the viscous properties of a fluid. Viscous drag can be further sub-divided into friction (or skin friction) drag and form (sometimes called viscous pressure) drag. Friction drag is equal to the shear stresses integrated over the vessel wetted surface; they are the result of the laminar and turbulent flow in the immediate vicinity of the vessel surface. For a deeply submerged vessel, the form drag is equal to the normal stresses (pressure) integrated over the instantaneous wetted surface. In an inviscid fluid, the pressure forces acting on a deeply submerged hull will integrate to zero. However, in a real fluid the pressure forces are non-conservative and will not integrate to zero. The net result is called the form drag; it results because the pressure distribution around the hull is modified by the presence of the boundary layer and separated region. For vessels operating on or near the free surface, the picture is further complicated because the wave drag is also the result of the pressure distribution over the hull. Consequently, there are direct links between the wave drag, form drag and friction drag.

While these links may not be strong, they may be very important from a design point of view. There are many examples of the interactions. A change in the hull shear stress by a drag reduction technique will alter the size and shape of the boundary layer. This in turn affects the pressure distribution over the hull form, resulting in changes in the wave resistance and form drag. Changing the shape of the hull will modify the pressure distribution over the hull, which will change the boundary layer and possibly the separation point location. The location of the separation point has a strong influence on the form drag and a lesser effect on the wave resistance. Surface waves generated by the ship cause local pressure oscillations that affect the stability of the boundary layer near the hull, also affecting the total friction drag. It should be noted that this discussion is for a ship moving at constant velocity along a straight path in calm water. All of the components of resistance will be modified by the unsteadiness associated with maneuvering or operation in waves.

Ideally, one would like to conduct an experiment with a model hull form equipped with an extremely high resolution array of shear stress and pressure sensors, integrating the results to obtain the skin friction drag and pressure drag. The wave drag can be determined by a wave cut analysis. Subtracting the wave drag from the pressure drag gives a value for the form drag. Unfortunately, this approach is neither practical nor technologically possible now. The traditional method of estimating the different drag components (wave, friction and form drag) will be discussed in the following section.

Secondary Drag: There are the additional components of drag that are usually neglected for normal ships operating at normal speeds, but they can become important in high-speed vessel operations. Spray drag and breaking bow waves can be a significant component for high-speed ships, particularly planning craft. This component of drag modifies both the pressure and shear stress distributions on the hull, but it eventually shows up as part of the momentum loss in the viscous wake. Similar to aircraft there may be an induced drag component due to dynamic lift acting on the appendages or the hull itself. Cavitation or ventilation drag may add or subtract from the total drag due to a reduction in the skin friction drag and an unequal increase in form drag. How the contribution of these components can be measured directly in model tests and scaled to full scale remains unresolved.

3 METHODS OF ESTIMATING FULL-SCALE SHIP DRAG

The ship design process is iterative, requiring many estimates of the hydrodynamic characteristics, such as calm water powering. In the initial design phases, obtaining a gross estimate quickly is probably more important than the accuracy. As the design is refined, the accuracy of the prediction becomes more and more important. For the designer, it would be beneficial if all the hydrodynamic characteristics could be accurately and quickly predicted from analytic and numerical methods. Unfortunately, the present state of the art is such that there is no method that is both fast and accurate. As the accuracy of the prediction method increases the cost and time required also increases. The most widely used methods involve *extrapolation* from both model test data and full-scale drag data obtained from ships of similar characteristics. Direct *computation* of ship powering requirements is a topic of continuing research.

Traditional Extrapolation Methods: Initial estimates of drag can be developed by extrapolating the values of several closely related ships. Empirical formulas based upon vast storehouses of ship design and sea-trial data have proved extremely useful in preliminary design. Widely used are the regression curves of Holtrop and Mennen (1982) for commercial vessels operating at conventional speeds. For high-speed craft, several standard hull form series provide accurate, empirically based design information: Series 62, hard chine planing hulls (Clement and Blount, 1963); Series 63, round bottom planing hulls (Beys, 1963); Series 64, high-speed displacement hulls (Yeh, 1965); and Series 65, long, slender planning hulls for hydrofoils (Holling and Hubble, 1974).

Drag is typically non-dimensionalized by dividing the drag force by $\frac{1}{2}\rho U^2 L^2$, where ρ denotes fluid density, and U is the vessel speed, and L is a characteristic length. In the field of naval architecture, the hull wetted surface area, S, is usually used instead of L^2.

$$C_D = \frac{Drag}{\frac{1}{2}\rho U^2 L^2} = f(\boldsymbol{R}, \boldsymbol{F}, \sigma, \boldsymbol{W}, \boldsymbol{M}) = f\left(\frac{UL}{\nu}, \frac{U}{\sqrt{gL}}, \frac{\Delta P}{\frac{1}{2}\rho U^2}, \frac{\rho U^2 L}{\tau}, \frac{U}{c}\right) \tag{1}$$

where (1) indicates that total drag is a function of the Reynolds number, $\boldsymbol{R} = (UL/\nu)$, Froude number, $\boldsymbol{F} = (U/(gL)^{1/2})$, cavitation number, $\sigma = (\Delta P/[2\rho U^2])$, Weber number, $\boldsymbol{W} = (\rho U^2 L/\tau)$, and Mach number, $\boldsymbol{M} = (U/c)$ (where U is the vessel speed, ν is the fluid kinematic viscosity, g is the gravitation acceleration vector, ΔP represents a pressure differential between free stream pressure and vapor pressure, L is some characteristic length, τ is the coefficient of surface tension, and c represents the speed of sound for the fluid).

Standard ship model testing only considers Reynolds number, $\boldsymbol{R}$, and Froude number, $\boldsymbol{F}$, with the effects of the other terms being negligible. However, during the course of the drag reduction investigation, it may become evident that the drag reduction materials (and ultimately, total drag) are affected, depending on local or global, Weber number, cavitation number, and/or Mach number as well. According to the principle of dynamic similitude, an exact scale (geometrically similar, or geosim) model experiencing a flow geometrically similar to that of the full-scale ship will have the same force coefficient. Unfortunately, it is not possible to conduct a scale model test where the Reynolds number scaled flow conditions and the Froude number scaled flow conditions are met simultaneously if gravity and the fluid are the same. Matching model and ship Reynolds number requires $U_s L_s/\nu_s = U_m L_m/\nu_m$, where subscript '$m$' denotes the model and subscript 's' denotes the full-scale ship. Since the $\nu_s \approx \nu_m$, it requires $U_m = U_s(L_s/L_m) >> U_s$. Matching model and ship $\boldsymbol{F}$ requires $U_s/(gL_s)^{1/2} = U_m/(gL_m)^{1/2}$. Hence, $U_m = U_s(L_m/L_s)^{1/2} << U_s$.

Froude was the first to resolve this dilemma and his method is still widely used. Since Froude demonstrated the validity of his method, additional methods have been proposed, the most widely accepted being Hughes' method. Both Froude's and Hughes' method utilize the assumption that the total drag can be separated into its components, and each component is dominated by a single scaling effect. A brief review both methods follows.

Froude's Method: Froude's method makes the assumption that total drag can be cleanly decomposed into friction drag and residual drag:

$$C_D(R,F) \equiv C_F(R) + C_R(F) \tag{2}$$

where C_F is the flat-plate friction drag coefficient (depending only on Reynolds number) and C_R is the residual drag coefficient (depending entirely on Froude number), consisting of the wave and form drag. Froude's method assumes that the friction drag coefficient of the wetted hull (for both the model, C_{Fm}, and ship, C_{Fs}) is the same as that of a flat plate of equivalent surface area at the same Reynolds number. The ITTC friction line (ITTC, 1957) is the most widely used estimate for the friction drag coefficient. The model is towed at a variety of speeds, recording for each speed the total model drag force coefficient, C_{Tm}. For each speed, the calculated flat plate equivalent friction drag, C_{Fm}, is subtracted from the total drag, resulting in the residual drag coefficient, C_R. This residual drag consists of wave drag and a significant amount of the form drag, and is assumed to scale with Froude number. The ship total drag, C_{Ts}, is the sum of the friction drag calculated from the flat plat friction extrapolation line, based upon full-scale ship Reynolds number, plus the Froude number-scaled residual drag, which was determined from the model tests. A final correlation allowance, C_A, is added to the actual full-scale ship drag coefficient, C_{Ts}. C_A relates the model calculated drag, C_{Tm}, to the full-scale ship drag coefficient, C_{Ts}, based on hull characteristics, to account for scaling inaccuracies, hull surface roughness, construction imperfections, etc.

$$C_{Tm} = C_{Fm} + C_R \tag{3a}$$
$$C_{Ts} = C_{Fs} + C_R + C_A \tag{3b}$$
$$\Rightarrow C_{Ts} = C_{Fs} + (C_{Tm} - C_{Fm}) + C_A \tag{3c}$$

Hughes' Method: Hughes' method is a variant of Froude's method, with an attempt to Reynolds number-scale the friction and a significant portion of the form drag, and *F*-scale just the wave drag. This is accomplished by towing the model at a slow enough speed such that there appears to be no waves generated, and considering the observed total drag as the sum of the friction and form drag, $(1+k)C_{Fm}$. The model friction drag, C_{Fm}, is estimated as previously mentioned, considering it the flat plate equivalent friction drag. The factor, k, represents the additional form drag as a fraction of friction drag that is Reynolds number-scaled, along with the friction drag. Typical values of k are $0.05 \le k \le 0.40$, for displacement ships. Typically, a Prohaska plot (Prohaska, 1966) is used to find the form factor. In a Prohaska plot, the low speed values of C_{Tm} are plotted against the values of F^4/C_{Fm} The y-intercept of the regressed data yields a value of $(1+k)$. Utilizing the form factor, k, implies that a significant portion of the form drag scales with Reynolds number, which may or may not be completely correct. The model is towed at successively higher speeds, and the additional drag above the calculated friction and form drag is considered the wave drag, C_{Wm}. As with Froude's method, the accuracy of Hughes' method is close, but not perfect, requiring a (different from Froude's method) correlation allowance, $C_{A'}$, to improve the estimate.

$$C_{Tm} = (1+k)C_{Fm} + C_W \tag{4a}$$
$$C_{Ts} = (1+k)C_{Fs} + C_W + C_{A'} \tag{4b}$$
$$\Rightarrow C_{Ts} = (1+k)C_{Fs} + (C_{Tm} - (1+k)C_{Fm}) + C_{A'} \tag{4c}$$

Figure 1 illustrates the relationship between the model and the full-scale ship drag for conventional model testing, using Hughes' method.

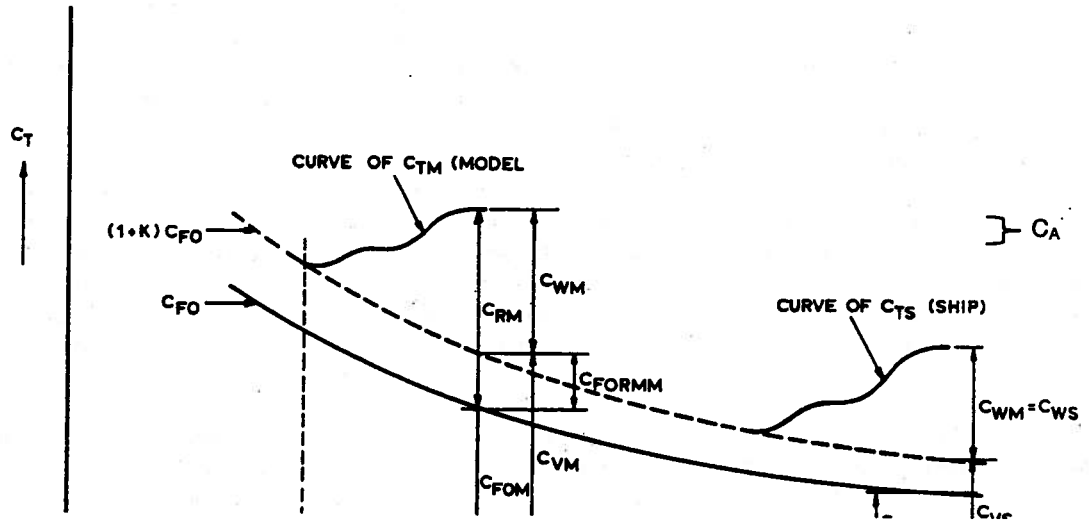

Figure 1: Extrapolation of model results to ship using Hughes' method, Van Manen, and Van Oossanen (1988)

There are several concerns with directly applying these traditional drag extrapolation techniques to high-speed ships. Neither of these methods account for spray drag, or large-scale ventilation drag. Froude's method scales the majority of form drag by Froude number-scaling, and Hughes' method appears to scale the majority of the form drag by Reynolds number-scaling. Given the fact that both methods require an empirically derived correlation allowance, C_A, or $C_{A'}$, to make the estimates come within an acceptable level of accuracy, it is possible that each method is scaling the form drag, (and possibly fractions of other components of drag) imperfectly. The value of C_A varies, depending on ship type and ship size, from approximately +0.008, to –0.002 (NAVSEA DDS 051-1, 1984).

The estimate of total ship drag is usually within 10 to 15 percent if the C_A is not utilized and within 2 to 5 percent if the C_A is utilized. It is also important to note that the skin friction line is an empirically derived friction correlation line, not necessarily representing pure skin friction. The ITTC 1957 model-ship correlation line is commonly used because it seems to deliver the best friction correlation between model and ship, not because it most accurately denotes actual skin friction. A modified experimental method and new scaling system may be required to more effectively scale the form drag.

Due to the large operational speed of high-speed ships, the model will have to be tested at relatively high speed to obtain scaled wave and spray effects. The relatively high model speed (compared to the more conventional slower speed model test) coupled with a relatively shallow towing tank could result in increased resistance due to depth effects. The larger the scale model tested, the greater the opportunity to achieving flow similitude with the full-scale ship. A (relatively large) 12 m long model of the 232 m full-scale ship that operates at 38.6 m/s (75 knots) would be required to run at Froude-scaled test speeds of up to $U_m = U_s(L_m/L_s)^{1/2} \approx 8.8$ m/s. The depth Froude number of a standard 10 m deep towing tank for this test is $U_m/(gh_{depth})^{1/2} \approx 0.89$, high enough to experience the increased resistance effects due to the restricted environment. Testing with a smaller scale model may mitigate this effect, however, inaccuracies from scaling friction and form drag would be magnified. The full-scale ship will also experience the depth Froude increased resistance effect if operating at high speeds while still over the continental shelf ((38.6 m/s)/(9.81 m/s^2 × 200 m depth)$^{1/2}$ = 0.87).

The scaling methods just discussed work well for conventional ships at conventional speeds, utilizing conventional propulsion. Due to our rudimentary understanding of how fluid drag reduction (FDR) methodologies may affect each type of drag, and their interaction, we're not yet prepared to conjecture how, or even if, the FDR effects can be scaled via one of the known methods. Because the interaction between non-conventional propulsion and hull flow can be large, the conventional methods of model testing, and scaling those results, will not work. Scaling high speed flow around the hull stern, including the effect of FDR will need to be investigated. These concerns don't eliminate the traditional methods from being utilized to assist in estimating the full-scale ship drag, but they do indicate the weaknesses that must be overcome.

Numerical Computation of Full-Scale Drag: There is a complete spectrum of numerical methods to predict ship resistance. From the computationally fast slender-body theories and Michell's integral to predict wave resistance to the three-dimensional and unsteady viscous computations that may take on the order of 1000 hours of super computer time. The accuracy of the prediction methods continues to improve with significant effort by hydrodynamicists, computer engineers and scientists. The most common of these advanced numerical methods are: Reynolds averaged Navier-Stokes (RANS) equations, large eddy simulation (LES), and direct numerical simulation (DNS). Each of these methods has strengths and drawbacks, as summarized in appendix B. As of yet, no computational numerical code has succeeded in predicting the hydrodynamic behavior (forces, pressures, velocities, etc.) of fluid flow around an entire hull form, or propulsion device, accurately enough to warrant entrusting the entire design process to these methods. However, these methods have produced valuable insight into the fundamental physics of viscous fluid flow, allowing us to begin seeking drag reduction solutions tailored to certain aspects of fluid flow. At present, the most significant benefit of computational methods may be the ability to predict the relative merits of competing, detailed appendage designs such as bulbous bows or water-jet inlets. Even though the absolute drag predictions are not accurate, knowing the relative merits of competing designs can greatly help the designer make important choices. As the speed and accuracy of the numerical methods increases, we expect to see more and more application to the entire design.

The most accurate method to predict full-scale resistance is still model testing. Model testing is relatively expensive and time consuming. If the promise of numerical prototyping a physical model within a few hours comes to fruition, then the time associated with model testing could be reduced to hours or days as opposed to weeks. The actually time in the model basin is short; it is the building of the model that takes the majority of the time and cost. As the previous section shows, scaling model test data to full scale has many challenges. The scaling process for conventional ships at normal speeds is well understood; with an appropriate correlation allowance the predictions should be within a few percent. For non-conventional hull forms and/or high speed the correlation becomes much more difficult and the accuracy of the prediction diminishes. For fluid drag reduction techniques, such as micro bubbles, the scaling laws are not even known. The most productive approach at the present time seems to be a combination of numerical and experimental approaches. Numerical methods are used to analyze many options and experiments are used to verify the results.

4 FRICTION REDUCTION THROUGH HULL-FORM OPTIMIZATION AND HULL SURFACE DESIGN AND CARE

The obvious solution to reducing total ship resistance is to reduce one or more components of drag, while not adversely affecting the other components of drag a comparable amount. Choosing ship hull characteristics such that they minimize the total wave energy for a given range of operating conditions reduces wave drag. Numerical analysis, full-scale testing and model experiments have introduced concepts such as increasing length to beam ratio, the bulbous bow, and the small water plane twin-hull (SWATH) form, as a means of reducing overall wave drag. Ensuring the hull is fair, and free of extraneous wetted appendages assists in reducing form drag. Maintaining smooth hull surfaces, through generally accepted construction processes, application of sea-worthy hull coatings, and routine hull cleaning and maintenance contribute toward minimizing friction drag. None of these existing methods will suffice in reducing the total drag enough to meet the operational requirements of a high-speed ship.

Optimization: Optimizing the hull form without geometric constraints to minimize wave drag can lead to design recommendations that are neither obvious, nor harmonious with form drag reduction, practical construction or operational requirements. Wyatt and Chang (1994) Hendrix, *et al.* (2001), Kuhn (2002), and Ragab (2003) detail methods for developing numerical optimization tools for developing a design that will reduce total drag. The efforts primarily focus on reducing wave drag, and rely upon a hybrid of potential flow theory to estimate wave drag, and several well-established empirical formulas for form and friction drag. These methods make the commonly used assumption that wave, form and friction drag can be modeled independently. However, the methods are qualitatively accurate in predicting how changes in the hull form will increase or decrease total drag. By positive and negative examples, the methods also demonstrate the importance of optimizing the entire system over a range of operational speeds, instead of a single speed, in order to avoid design extremes and inefficiencies at non-optimized speeds. They also show the importance of considering all three conventional components of drag in the optimization analysis. The analyses also conclude that a hull form could be optimized to significantly reduce wave drag at the expense of adding a lesser amount of form drag. A brief review of Hendrix, et al.'s optimized hull form will lead most designers to the conclusion that they may not be suitable for a traditional engine room, auxiliary machinery, or cargo layout. This points out that additional constraints applied to the parametric representation of the hull form shape will be needed in order to produce an optimized hull form that will accommodate mission and machinery space constraints as well as integrated hull form constraints (fixed displacement, LCB location, etc.), issues that Wyatt and Chang, and Kuhn have taken into account.

Significant value can be added to the final design by performing numerical analysis to optimize the hull form. In the future, optimization models will need to more tightly couple the effects of wave, form, and friction drag, as well as induced and spray drag in order to be a more effective tool in the design process. The algorithms necessary to support the numerical modeling require fundamental research, coupling theoretical fluid dynamics with laboratory results. However, it is unlikely that hull form optimization alone will ever be able to provide the factor of two reduction in resistance that will be required to produce operationally effective high speed transport. (Over a limited range of moderate speeds where wave resistance dominated, Wyatt and Chang (1994) achieved a theoretical 80 percent reduction in wave resistance; a 50 percent reduction in measured wave pattern resistance; and a 25 percent reduction in full-scale effective power, based on model test results.)

Surface Design and Care: The hull wetted surface imperfections must be minimized during design and construction. Also, the environmentally induced flaws (scratches, gouges, bumps, etc.) and fouling must also be minimized, by improved design, or maintenance process. High performance racing craft have very precise, very smooth hulls. The high speed logistics ship hull will be required to maintain the precision and cleanliness of a racing hull, applied to a hull a couple of orders of magnitude greater in size, challenging existing construction and maintenance techniques.

Hull fouling by marine organisms represents one of the most significant obstacles to a well designed and constructed hull form from obtaining its maximum design speed. Analysis of operational ship data indicates that after 4 to 5 months of service (following a total hull cleaning) ships can expect to require 10 percent more power to obtain design speed, and after 1 year of service, require up to 30 percent more power (SNAME Technical & Research Report R-18, 1975). The added friction due to fouling is on the same order that we are striving to eliminate through advanced fluid drag reduction technology. Interestingly, the adverse effects of marine fouling on ship speed can be significant, even before the marine fouling is visible to the unaided eye. Care will be required to ensure that

the fluid drag reduction technology is compatible with the minor amounts of marine fouling expected during normal operations, and that the hull cleaning method is compatible with the technology; e.g., polymer ejection is still effective with small amounts of fouling present around the nozzles, and sand blasting or chemical cleaning the hull doesn't degrade the ejection nozzles.

5 TURBULENCE IN A HIGH REYNOLDS NUMBER BOUNDARY LAYER

Distances in viscous flow are usually measured using non-dimensional "wall-units", which are denoted by the "+" superscript. Distance from the wall, normal to the wall, is defined as $y^+ = yu_\tau / \nu$, the non-dimensionalized distance from the wall, based upon the fluid kinematic viscosity, ν, and the wall-friction velocity, $u_\tau = (\tau_w/\rho)^{1/2}$ (sometimes denoted as u^* or u_*). Very near the wall, $y^+ \leq 5$, the boundary layer is dominated by viscous shear, and this region is defined as the viscous sublayer. This region is extremely resistant to turbulent velocity fluctuations, and virtually all stress is due to viscous shear of the laminar flow. Outside this viscous sublayer is the overlap layer, located $5 \leq y^+ \leq \sim 300$ (and possibly beyond). The overlap layer is usually divided into two regions: the buffer layer, directly above the viscous sublayer, located $5 < y^+ \leq \sim 30$; and the logarithmic layer, located $\sim 30 < y^+ \leq \sim 300$. Large scale turbulent structures dominate the outer region.

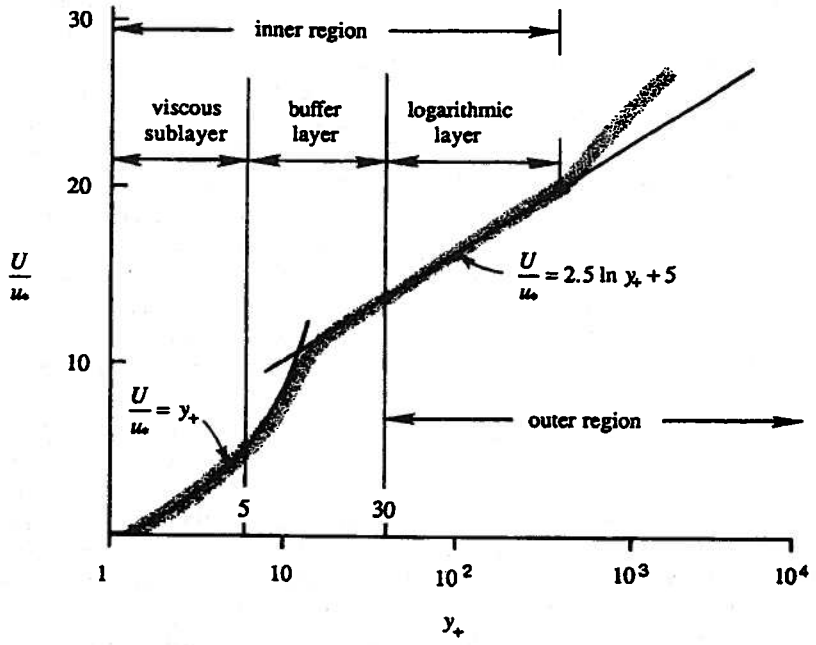

Figure 2: Near-wall flow magnitude: Law of the wall, Kundu, and Cohen (2002)

Experimental turbulent flow measurement techniques and instrumentation have improved during the last decade, allowing researchers to observe patterns of turbulent flow that were previously generalized by simplistic mathematical equations. Very-fine scale direct numerical simulation (DNS) computer modeling of the Navier-Stokes equations have been conducted, and these results corroborated with observations from experiments. There is still conjecture about precisely which mechanism(s) initiate and regenerate the turbulent behavior, and exactly how all of the observed dynamic flows interact. However, there is enough experimental and numerical evidence to support a general agreement that turbulent flow is dominated by the following mechanisms: 1) streamwise "streaks" of low-speed streamwise vortices; 2) packets of hairpin-like vortices; 3) "bursting" of the low-speed fluid into the outer layer; and 4) higher speed outer layer fluid "sweeping" into the lower region to maintain continuity. Smith (1998) lays out the following conceptual model for the initiation and regeneration of turbulence.

Once the vortex deformation develops, most likely due to transition of a laminar boundary layer, or from external vorticity contamination, hairpin-like vortices will develop in the shear layer near the surface. Once

these three-dimensional vortices are present, they are able to (1) regenerate new vortices through an interaction with the viscous wall layer, (2) interact with other three-dimensional vortices to yield larger-scale flow structures, and (3) facilitate the transfer of energy and momentum within the turbulent boundary layer.

The low-speed streaks are generated by the interaction of a passing streamwise or hairpin-like vortex with near-wall fluid creating a narrow "streak" of low-speed fluid that lifts away from the wall as the streak moves downstream. This lifting away is sometimes referred to as "lift-up". The average spanwise spacing between the streaks is approximately 100 wall units. These flow patterns are primarily located very close to the surface, $y^+ < 25$, although measurements by Meinhart and Adrian (1996) indicate that low speed streaks are not limited to the buffer layer, but can extend up into the outer as well. The regularity in spanwise spacing seems consistent over a broad range of Reynolds numbers ($103 < R_\theta < 106$, where $R_\theta = u\theta/\nu$, and θ is the boundary layer momentum thickness), but this regularity deteriorates rapidly with distance from the wall surface. Adrian and Balachandar (1998) indicate that it is the cooperative effect of aligned hairpin vortices pumping fluid in the Q2 (second quadrant of a u', v' map, i.e. $-u'$ and $+v'$, where u' and v' are defined as the deviation of the time-averaged velocities, u and v for a given time period) direction that assist in producing the very long (1000 wall units) low-speed streaks.

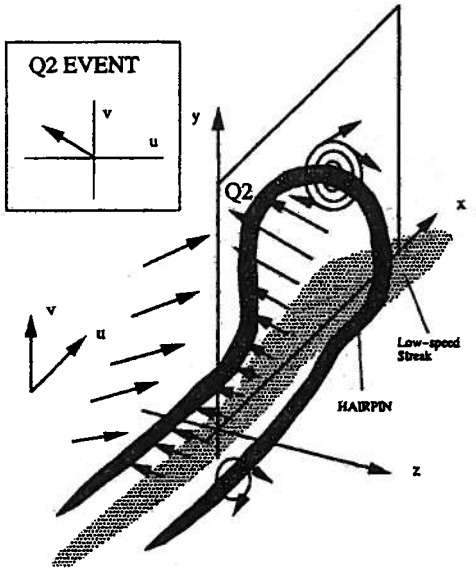

Figure 3: Q2 lift-up event (Hoyt 1998)

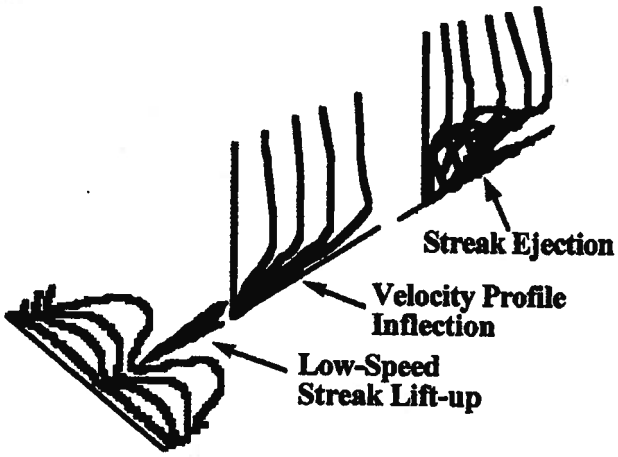

Figure 4: Streak ejection process (Smith 1998)

If the original vortex is strong, it can precipitate a burst event, by a streak in proximity to the strong vortex becoming unstable, and rolling up into a secondary hairpin-like vortex, ejecting a portion of the streak into the outer region. If the vortex is weak, a streak may form but not evolve into a hairpin vortex. The streak may diffuse or be acted upon by subsequent vortices.

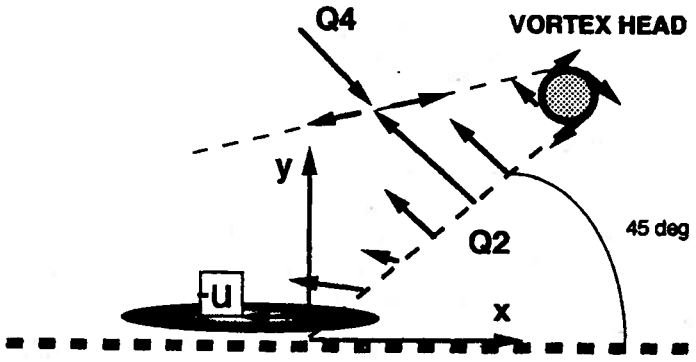

Figure 5: Schematic of a hairpin vortex and associated flow field properties that form the signature of a hairpin in the *xy*-plane (Adrian and Balachandar, 1998)

Adrian and Balachandar (1998) contend that the symmetric hairpin-like vortices stack up in the streamwise direction, one behind another. The adjacent hairpin-like vortices within a packet result in strong internal shear layers where the Q4 ($+u' -v'$) down-flow from the upstream vortex head meets the low-speed Q2 ($-u' +v'$) up-flow by the downstream vortex. Experimental evidence and computational results indicate that asymmetric, cane-shaped, one-sided hairpin vortices occur more frequently than the symmetric, omega-shaped hairpin vortices.

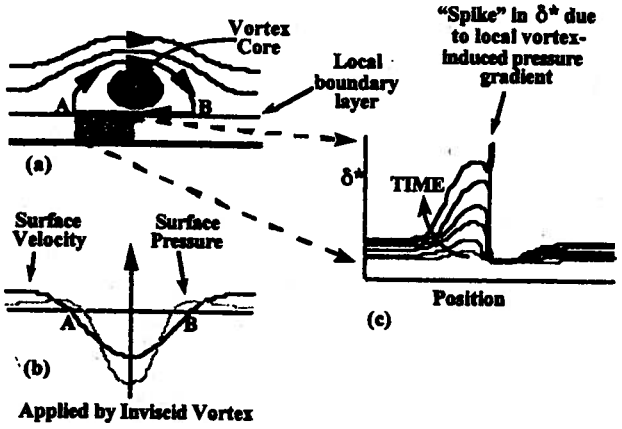

Figure 6: Schematic of the generic interaction of a vortex in close proximity to a surface with the viscous wall layer (Smith 1998)

A "burst" is the rapid ejection of a streak into the outer region of the boundary layer; essentially a form of localized unsteady separation. Smith (1998) contends that this is due to a local adverse pressure gradient created by an advecting wall-region vortex. This burst can result in one or more hairpin-like structures in the immediate wake of the initial vortex. A "sweep" is a three-dimensional inflow of high-speed fluid from the outer region toward the wall, because of the preceding burst. The incoming fluid will initially impinge near the plane of symmetry of the low-speed streaks, and then will be induced toward the wall, creating a "sweep" maneuver.

The cyclical "streak-liftup-hairpin-burst-sweep" turbulence model allows us to consider targeting specific physical areas or mechanisms of turbulent flow for drag reduction purposes. Currently, it is believed that interrupting, stabilizing or delaying the onset of any one of these mechanisms, would suppress the turbulence, and hence, overall friction. For example, optimized longitudinal riblets have been shown to reduce overall friction by up to 10 percent. Smith (1998) asserts that the riblets inhibit spanwise flow near the surface, reducing the capacity of the wall-region vortices to generate low-momentum streaks, and that polymer injection into the near-wall region appears to stabilize the streak formation, as evidenced by wider streak spacing, and reduced bursting activity. Polymer injection may either affect the streak directly, by inhibiting spanwise unsteady pressure gradient induced by the hairpin vortices, or indirectly, by providing a region which is locally more viscous, damping the external perturbations.

The preceding description of turbulence generation has been based upon experimental and computational observations of flat plates, with little or no pressure gradient, at relatively low Reynolds numbers. It may not be prudent to extrapolate the behavior of all of these turbulence generation mechanisms to very high speeds over curved bodies, with an adverse or oscillating pressure gradient (or sheet cavitation), in a contaminated fluid. Additional fundamental investigations into the mechanisms of turbulence generation needs to be performed and under the harsh stochastic conditions that a high-speed ocean-going vessel would encounter.

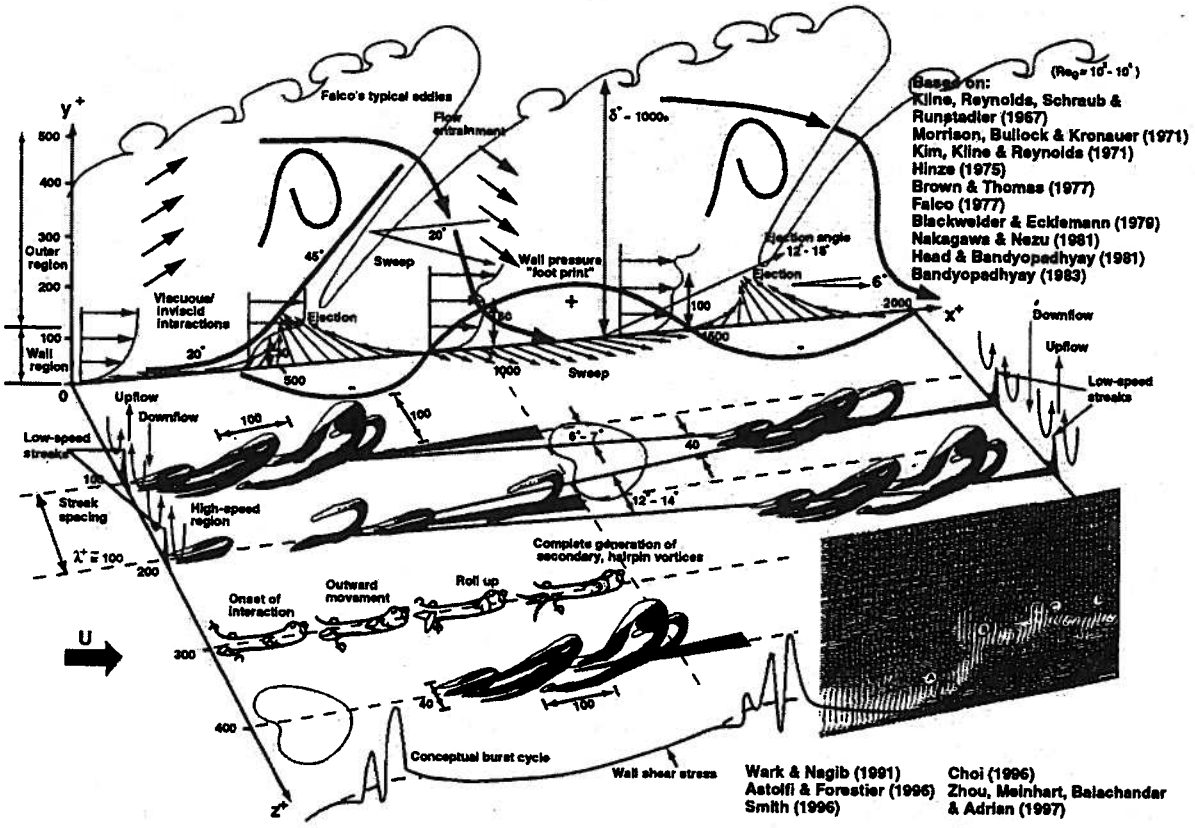

Figure 7: Conceptual turbulent boundary layer near-wall phenomenology, Meng (1998)

6 FRICTION DRAG REDUCTION (FDR) TECHNOLOGIES

During the past few decades FDR techniques have been researched and applied throughout the aviation and naval communities, the petroleum industry, and many other industries in a host of applications. The results of the applications have been mixed.

Table 1 summarizes the research results from across a variety of FDR approaches, showing the result with the most relevant geometry and/or the highest test speed. Note that this table represents a "snapshot" of various test results, not the average result due to the application of these various techniques. A more detailed summary of this information is available in Appendix A.

FDR Type	% drag reduction	Tested body geometry	Test Speed	Test Conditions	Other geometries tested
Riblets	< 10%	0.5 x 4 m flat plate	Re < 5000	Steady flow, zero pressure gradient, smooth surface, fresh water	pipe, torpedo shape
Compliant Walls	< 7%				
Ventillation	< 12%	14.0 x 84.6 m barge hull			
Ventillation & water repellent surface	< 55%	flat plate	8 m/s		model ship
Microbubbles	< 65%	0.35 x 2.73 m flat plate	7.6 m/s	Smooth plate, salt water	axisymmetrical model, pipe
Polymers	< 60%	0.4 x 1.85 m flat plate	Re < 1.7E7	Smooth plate, fresh water	pipe, model ship
Polymers & Microbubbles	< 85%	0.15 x 0.3 x 12.0 m model ship	< 6 m/s	Steady flow with free surface effects, smooth surface, fresh water	
Surfactants	< 60%	0.04 x 5.0 m flat plate	Re < 5000		pipe
Fibers	< 94%	0.024 to 0.070 m dia. pipe	Re < 2.0E5	Fibers suspended in a polymer solution	
High Viscosity Fluid	< 60%	0.05 x 0.27 m flat plate	< 10.2 m/s	Steady flow, positive pressure gradient, smooth surface, fresh water	
Wall Oscillation	< 45%	0.5 x 0.5 m flat plate	< 2.5 m/s	Steady flow, zero pressure gradient, smooth surface, air	
Blowing/Suction	< 25%	flat plate	ReD = 1800 and 3300	DNS model	
Electrokinetics	< 5%	0.075 x 1.0 m axisymmetric model	5.5 m/s	Smooth, salt water	

Table 1: Fluid drag reduction technology test performance summary

The vast variety of FDR technologies can be categorized by their approach to drag reduction, but the way these technologies are categorized is somewhat arbitrary, given that our main interest is how to most effectively influence the mechanisms of turbulent generation. Techniques from different categories have been combined, sometimes revealing impressive, if little understood, synergies. Mochizucki and Osaka (1998) note that there can be significant difficulty in determining the actual effect of a particular FDR technology upon the mechanism of turbulence generation. For instance, in most experiments, the wall shear stress was determined by indirect methods assuming similarities in mean quantities (e.g. u'^2, or $u'v'$, etc., an issue of resolution or scale) or estimated from results provided by other studies. In addition, mathematical models of the kinematics of the coherent turbulent structure have been assumed to be, until recently, relatively simple, whereas in reality, the dynamics of the quasi-periodic, three-dimensional vortical motions can hardly be described by well-defined mathematical equations.

The potential for very high drag reduction exists due to synergy between FDR technologies: polymer and microbubbles (Phillips, *et al.*, 1998), polymer and fibers (Metzner, 1977), microbubbles and repellent coating (Fukuda, *et al.*, 2000), etc. However, it can be difficult to assess the optimal synergy between the FDR technologies until we more thoroughly understand how each technology directly affects each mechanism of turbulence generation. A significant amount of effort during the past decade has brought forth a better, if incomplete, understanding of the relationship between FDR technologies and the turbulence generation mechanisms. The following section attempts to provide a brief description of each FDR category, and how it may interact with the mechanisms of turbulence generation.

Compliant Walls: The primary intent of compliant wall technology is to take advantage of constructive fluid-wall interaction to delay or negate the onset of turbulence. Preliminary research in this field was inspired by observations that many marine animals seem to be capable of swimming much faster than their inherent propulsion power should allow. This led to the idea that these marine animals not only have optimized shapes, but also have optimized skin surfaces that delay the onset of turbulence, reducing overall drag (Krämer, 1960 and 1962). Compliant walls are

generally constructed with a relatively thin, moderately stiff surface layer laminated over a thicker layer(s) of much softer, elastic material. Many variants of this theme have been tried.

Überall and Madigosky (1998) and Gad-el-Hak (1998) summarize the four fluid-wall instabilities that need to controlled through appropriate use of materials:

- Tollmien-Schlichting (T/S) waves: unstable waves on a rigid wall that appear in the laminar-turbulent transition region; these waves can be stabilized by changing the wall from rigid to compliant
- Compliance-induced flow instabilities (CIFI): can appear in addition to T/S waves even if the wall is compliant; this instability is essentially induced by resonance, where the flow speed is close to the natural speed of the surface waves of the compliant wall material
- Kelvin-Helmholtz instability: arises out of a combination of T/S waves and CIFI
- Static Divergence: observed in the form of very slow moving, large amplitude waves in the compliant wall material, resulting in a dramatic increase in drag

All four of these instabilities can lead to (traveling wave or standing wave) "flutter" on the compliant wall; high speed, small amplitude waves that precede turbulent flow. The difficulty in controlling all four types of instabilities simultaneously is that techniques that reduce one type of instability can exacerbate another, for a given flow speed, and downstream location.

Carpenter (1998) has conducted a significant amount of laboratory and numerical research on compliant coatings/walls. Based upon his numerical analysis of an optimized compliant wall system, he contends that it is theoretically possible to indefinitely delay the onset of the instabilities that lead to turbulent flow. The experimental evidence to support this theory is inconclusive (Carpenter, 1998). Choi, *et al.*, (1997) reported a small amount of drag reduction (up to 7 percent) with a relatively stiff, single layer viscoelastic compliant wall. Carpenter's (1998) analysis of this result indicates that for stiffer compliant walls, the turbulent flow induces quasi-random displacements in the compliant wall. These displacements in the compliant wall in turn affect the near-wall turbulent structures that trigger the turbulence cycle. These results are similar to the drag reduction obtained from randomly placed roughness elements on the surface of a rigid wall.

Riblets: Riblets, or micro-grooves, are longitudinal micro-grooves machined into the surface, or micro-ridges placed onto the surface by an appliqué. The machined grooves may be square-cut or v-cut, and there may be lateral grooves in addition to the longitudinal grooves. The height (depth) of the riblets vary, with $y^+ < 5$ being typical. Recently, research into three-dimensional surface roughness has yielded results similar to that of riblets.

Experiments with riblets , in both air and water have demonstrated a skin friction reduction of 8 to 10 percent (Mochizucki and Osaka, 1998). Drag reduction of approximately 8 percent has been observed for plates, torpedo shaped bodies and the interior surface of pipes if the riblets are tailored to specifically match flow conditions (Hoyt, 1998).

The primary effect of riblets appears to be interfering with lateral fluid motion near the wall, which is believed to trigger the low-speed streaks lifting up, beginning a turbulence cycle. The transverse spacing between riblets appears to be the critical dimension, with the lateral distance in wall units, $\lambda^+_z \approx 100$ being optimum. Riblets mitigate the lateral momentum transfer that occurs immediately following the low-speed streak lift-up. It acts as a type of wall that prevents many, but not all, of the laterally projecting streaks from providing the perturbation necessary to initiate the turbulent generation cycle in an adjacent fluid parcel. During the conditions of maximum drag reduction in the presence of riblets, Wang, *et al.* (2000) observed a thickening of the viscous sublayer by approximately 10 percent, and a reduction of the average lateral distance between low-speed streaks, λ^+_z, by approximately 20 percent.

Ventilation: Latorre (1997) conducted model and full-scale experiments with ventilation, injecting air into a shallow cavity at the bottom surface of the hull. Air ventilation resulted in a net drag reduction of 15 to 18 percent for the model tests and 10 to 12 percent for the full-scale hull. A blower was used to generate the ventilation airflow, requiring only 2 to 3 percent additional power to generate the 10 to 12 percent drag reduction.

Fukuda, *et al.* (2000) demonstrated that a super water repellent coating, combined with a very thin air film resulted in a peak skin friction drag reduction of 80 percent at 4 m/s and 55 percent at 8 m/s. The super-water-repellent (SWR) coating/air film combination was tested on several different test configurations, including a flat plate, square pipe, tanker model and a "pencil" (long, skinny) ship model (obtaining up to 85 percent friction drag reduction). All test platforms demonstrated drag reduction proportional to the amount of surface area that could effectively utilize the combination of the SWR coating and the air film (the bottom side of the plates and the ship

models). The technology demonstrated itself to be very simple to employ, and requires low energy cost to generate the air film.

The data seems to indicate that SWR technology becomes less effective as speed increases, leading to the question of how high a speed this technology could be effectively employed. The technology may be made more effective at higher speeds through the application of increased airflow and/or and improved SWR coating.

No turbulent flow drag reduction mechanism was discussed in either paper. However, one may hypothesize that these systems do not actually suppress any of the mechanisms of turbulence, but rather take advantage of a significantly reduced dynamic viscosity, μ_{eff}, with a value somewhere between that of water (~1.0×10^{-3} kg/m·s at 20°C) and air (~1.8×10^{-5} kg/m·s at 20°C), which is approximately 55× lower. A μ_{eff} only 3-4× lower than that of μ_{water} could easily account for the skin friction drag reduction, due to the shear stress at the wall, $\tau_w = \mu_{eff} du/dy$, evaluated at the wall. The SWR coating seems to improve the surface's ability to "hold" the air film, improving the air lubricating capability. For a ship with either buoyant or dynamic lift, one must question how the vessel will be supported if there is a full layer of air—will have to be at the ambient water pressure.

Microbubbles: Microbubbles are very small bubbles, with non-dimensional diameter, D^+, on the order of 100 to 250 wall units, where $D^+ = Du_\tau/\nu$. The effect of microbubbles is not to be confused with the effect of the near-total ventilation of the wall surface.

Under laboratory conditions up to 85 percent (and higher) friction drag reduction has been achieved. Guin, *et al.* (1998), conducted experiments, and reanalyzed data from experiments previously performed by Madavan, Deutsch, and Merkle. Their investigation concluded that drag reduction is most heavily influenced by the concentration of microbubbles within $y^+ \leq 150$, representing the inner boundary layer region. Guin, *et al.*, contend that the microbubble effect can be viewed as the cumulative effect of each individual microbubble within the inner region. The magnitude of drag reduction is related to an effective bubble passing frequency, ω^+_b, where $\omega^+_b = \omega_b \nu / u_\tau^2$, with $\omega_b = 2\pi(\alpha_w U_m / D_b)$, where α_w is the local void fraction near the wall, and U_m is the fluid bulk velocity. This effectively converts the fraction of gas near the wall to a frequency of near-wall velocity perturbations. The correlation between ω^+_b, and drag reduction could imply that high frequency excitation near the wall is responsible for inhibiting mechanisms of turbulence generation. However, it is not understood how microbubbles interact with one or more of the turbulence generation mechanisms to mitigate turbulence generation. Meng and Uhlman (1998) hypothesize that bubble splitting within the inner region may act as a turbulent energy absorption mechanism. They don't discuss which turbulent generation mechanism(s) may be affected. However, one may conjecture that the bubble splitting would absorb energy passing through the inner region, supressing the lift-up or sweep mechanisms.

Persistence, or the duration that microbubbles remain close to the wall, has a significant impact on the overall effectiveness of microbubbles for drag reduction. Madavan, *et al.* (1984), note that the effectiveness of microbubbles on drag reduction declines by 50 percent over a streamwise distance of 25δ, where δ is the effective boundary layer thickness. This may be due to: the growth of the boundary layer thickness, effectively reducing the local void fraction; bubble diffusion away from the wall; or bubble coalescence and subsequent rise away from the wall due to buoyancy. Salt water or seawater seem to have a beneficial effect on microbubble size and persistence. For a given microbubble generating system (nozzle) and flow conditions, microbubbles formed in salt water will be smaller and have greater persistence than those formed in fresh water. Meng and Uhlman (1998) identify three basic physical mechanisms that may cause the smaller bubbles in salt water: reduced surface tension between the gas bubble and the water; an organic film; or a metalionic film.

Polymers: Certain long-chain polymers, added to a flow stream in concentrations as low as 0.2 wppm (Warholic, *et al.*, 1999), have demonstrated significant drag reduction. Increasing the polymer concentration generally increases the drag reduction, up to a certain limit (Ptasinski, *et al.*, 2001). Individual polymer strands in an equilibrium state can be thought of as small, coiled "balls" of polymer. A Newtonian fluid such as water exhibits the characteristic that the shear stress due to a strain rate is equivalent regardless of the direction of the strain. Adding long chain polymer to the fluid seems to change this isotropic property to an anisotropic one, by reducing the shear stress in the streamwise direction, depending on the flow characteristics.

Koskie and Tiederman (1991) investigated the behavior of long chain polymers in boundary layers, and sought to discern the particular mechanisms of turbulence generation that the polymer solution affected. They concluded that strong extensional streamwise motions, u', in the flow stretch the polymer molecules, resulting in the bulk of the fluid in this region having anisotropic stress properties that dampen small-scale motions in the flow. However, the strong extensional streamwise motions remain unchanged in the presence of the polymer. The average turbulent burst period in the polymer laced boundary layer increases, as does the streak spacing. The presence of polymer

appears to ultimately reduce the number of low-speed streak structures in the flow, but does not seem to affect the behavior, or consequences, of the burst, once the burst has been initiated.

Within a zero pressure gradient, Newtonian fluid boundary layer (no polymer), there will be virtually constant stress, τ, from $0 \le y^+ \le 250$, where

$$\tau = \mu \frac{d\overline{u}}{dy} - \rho \overline{u'v'} \tag{5}$$

Viscous stresses dominate for $y^+ \le 5$, Reynolds stresses dominate for $y^+ \ge 250$, and a combination of these apply in between. Injecting polymer into the boundary layer results in a stress "deficit" in the region $6 \le y^+ \le 100$ and the above equation is no longer valid. Koskie and Tiederman (1991) assert that polymer has this effect within this region due to the flow being extensional. Flow is not extensional for $y^+ \le 5$ due to the viscous sublayer exhibiting completely laminar behavior. Beyond the buffer region, for $y^+ \ge 100$, the extensional motions are much weaker than those in the lower region. Under the influence of the polymer, the Reynolds stress term is reduced due to a lower $\overline{u'v'}$, however the magnitude of the individual large amplitude fluctuations, u' and v', is not reduced. While the magnitude of the peak u'^2_{RMS} remained unchanged in the polymer solution flow, its position moved further away from the wall.

Warholic, *et al.*, (1999) achieved similar results, and further noted that the logarithmic layer is displaced outward, and the thickness of the viscous sublayer increases as drag reduction increases. The displacement of the location of the peak u'_{RMS} value outward seems to directly correspond to the increased thickness of the viscous sublayer. As the polymer concentration in the boundary layer is increased, the drag reduction increases, and the $\overline{u'v'}$ term decreases throughout the water column of the boundary layer (all y^+ in the boundary layer). For very high levels of drag reduction, the velocity profile within the boundary layer no longer has a logarithmic relation, and $\overline{u'v'} \approx 0$ throughout the water column. Ptansinski, *et al.*, (2001), as well as others, note that at high polymer concentrations (> 400 wppm) the actual drag reduction can exceed Virk's theoretical maximum drag reduction. This may indicate that for high polymer concentrations, more than one turbulence mechanism is being favorably affected.

Large differences in the magnitude of drag reduction are observed depending on the type of polymer used and the way it is applied to the boundary layer. Polymers that are more effective for slower speeds are not necessarily effective at higher speeds, and vice versa. Polymers, and their effectiveness, are rapidly degraded by the shearing forces within the boundary layer, and the polymer must be continually seeded into the boundary layer to maintain the drag reduction effect.

Surfactants: Surfactants are complex molecules with hydrophilic and hydrophobic ends that permit self-assembly into micelles, long chains, and layered structures. These long chains are torn apart by strong shear forces, but the nature of the surfactant permits it to reassemble under more favorable conditions. Due to their ability to remain effective after passing through a turbulent pumping system surfactants are frequently used for drag reduction in circulating fluid systems. Theoretically, surfactants can exceed the maximum drag reduction obtainable using polymers (Dimotakis, *et al.*, 2000).

In the presence of surfactants, the boundary layer behaves very much as if it were being affected by polymer so that $\overline{u'v'} \approx 0$ throughout the water column. While the magnitude of the individual large amplitude fluctuations, u'/u_τ and v'/u_τ were not much reduced, the location of the peak u'_{RMS} shifts outward (Kawaguchi, *et al.*, 2002). Generally, drag reducing surfactant solutions demonstrate viscoelastic flow behavior, and it is widely believed that the characteristic of viscoelasticity provides the drag reduction capability, differing from polymers, which provide drag reduction through the effect of extensional viscosity.

Lu, *et al.*, (1997) investigated a surfactant solution that did not exhibit normal viscoelastic behavior, and had very high extensional viscosity. The investigation concluded that a high ratio of extensional viscosity to shear viscosity correlates well with drag reduction effectiveness. Reevaluating previously obtained data for surfactant solutions supported these findings. Lu, *et al.*, (1997) conclude that the mechanism of surfactant drag reduction is likely due to the suppression of small-scale turbulent eddies. The large-scale bursts remain, where extensional motions are large. However, in the presence of a surfactant solution, the dissipation of the high frequency energy resulting from the bursts is significantly increased, reducing the turbulence generation initiation mechanism.

High Viscosity Fluid Layer: Kato, *et al.* (1993) demonstrated that a high viscosity fluid injected at the wall, in the direction of fluid flow reduces friction drag. The fluid density changes with distance normal to the wall, from a low-

viscosity fluid next to the wall in the viscous sublayer, to a high-viscosity fluid in the buffer layer, and back to a low-viscosity fluid in the outer layer (and above). Friction drag is a function of shear stress near the wall. Shear stress, as previously defined in equation (5) is a function of the local streamwise velocity gradient and Reynolds stresses. Kato, *et al.* (1993) surmised that the high viscosity fluid reduces the intensity of the Reynolds stresses in the buffer region, resulting in an increase in the local velocity gradient. This increase causes a reduction of the velocity gradient in the viscous sublayer, resulting in reduced wall shear stress. They recognize that some of the drag reduction is likely due to the increased momentum of the injected fluid. Experiments with injecting plain water through the same mechanisms indicate that the contribution of increased momentum may be limited to approximately 10 percent.

Spanwise Fluid Oscillations: Spanwise oscillation of the fluid is a superposition of "Stokes 2nd Problem" onto an otherwise normal turbulent boundary layer flow.

Direct numerical simulation (DNS) investigations by Akhavan, *et al.*, (1992), Baron and Quadrio (1996) and Coleman, *et al.*, (1996) indicated that plate skin friction drag could be reduced by inducing spanwise oscillatory flow. The Akhavan, *et al.*, (1992) study indicated that it made no difference whether the wall was oscillated over a steady flow, or if the wall was fixed and the fluid was oscillated.

Optimal results were obtained for an oscillation period of $T^+_{osc} \approx 100$ (where $T^+_{osc} = T_{osc} \cdot u^2_\tau / \nu$) and a spanwise flow rate of $0.8 Q_x \sin(\omega t)$ (where Q_x is the flow rate per unit width in the streamwise direction). These optimal parameters reduced the skin friction drag by 40 percent. The oscillatory flow also showed a 40 percent reduction in the $-\overline{u'v'}$ Reynolds stress, and a reduction of the peak velocity fluctuations: w', by 35 percent, v', by 30 percent, and u', by 14 percent. Reducing the spanwise flow rate resulted in less friction drag reduction. Oscillatory flows at periods much above and below $T^+_{osc} \approx 100$ also resulted in less friction drag reduction.

Choi and Clayton (1998) followed up with an oscillating wall laboratory experiment. Their results confirmed the DNS investigation results, showing the boundary layer logarithmic velocity profile is shifted upward, and obtaining a reduction in skin friction drag as high as 45 percent. Their results also show a reduction in the mean velocity gradient, demonstrating a reduced wall shear stress, and the inner-scaled velocity profiles show that the linear region of the viscous sublayer is increased from $y^+ \approx 2.5$ to $y^+ \approx 10$ at the maximum oscillation frequency of 7 hz. The lab experiments also show a reduction of the lower frequency (< 50 hz) turbulent energy, and an increase of the higher frequency turbulent energy, indicating energy transfer. Choi and Clayton (1998) conclude that drag reduction strongly relates to the net spanwise vorticity generated by the oscillatory flow. This additional spanwise vorticity realigns many of the longitudinal (streak) vortices back into the spanwise direction, reducing the near-wall burst activity. Thus the spanwise oscillatory flow interrupts and suppresses the turbulence generation cycle.

Blowing, Suction, and Induced Body Forces: Active control by blowing and/or suction attempts to directly counteract the wall-normal velocity turbulence events (streak lift-up and burst and/or the subsequent sweep phenomena) by using flow nozzles, electro-kinematics, or electro-magneto-hydrodynamics. Alternatively, uniform blowing seems to lower skin friction drag and increase velocity fluctuations, and uniform suction seems to have a nearly opposite effect.

Choi, *et al.*, (1994) conducted a series of DNS investigations, controlling the v-component of velocity in response to turbulent structures for a variety of detection and response schemes. The turbulent structure detection sensors were placed above the wall surface at a height of y_d. A counteracting v blowing or suction velocity was applied depending upon whether the turbulent structure velocity exceeded the predetermined threshold value, v_{th}.

The DNS study achieved a 25 percent friction drag reduction (compared to a theoretical maximum reduction of 65 percent for laminar flow) for a sensor $v_{th} = 0$ (maximum sensitivity), and $y^+_d = 10$ (where $y^+_d = y_d \cdot u_\tau / \nu$). Friction drag substantially increased for $y^+_d = 26$, and drag reduction was significantly reduced for $y^+_d = 5$. Increasing the v_{th} (reducing the detector sensitivity) resulted in a corresponding reduction in drag reduction (below 25 precent). Placing the turbulent structure sensors into the flow was easy, and convenient for the DNS investigation, but would not be practical for and actual, physical system. Choi, *et al.*, (1994) developed an algorithm to correlate the turbulent structures of the outer region ($y^+ > 10$) to the motion sensed at the wall surface. The DNS investigation was run with the sensors at the wall surface, and anticipating the blowing and suction that should be introduced via the control algorithm. Utilizing this control scheme, the friction drag reduction dropped to 6 percent, similar in effectiveness to the passive riblets technology.

Laboratory experiments, as reported by Meng (1998), and conducted by O'Sullivan and Biringen (1998), demonstrate the difficulty in transporting the physics observed in the DNS studies to actual, physical experiments. O'Sullivan and Biringen's experiment utilized electro-magneto-hydrodynamic micro-tile actuators to induce a Lorentz force, providing v-component velocity control. They utilized the Alfredsson and Johansson (1984)

experimental method for determining turbulent structures, or events, that should be counteracted. The system produced localized deviations in skin friction on the order of 15-18 percent, and the average skin friction within the control volume changed by ±4 to 5 percent. However, there was virtually no change in the mean wall shear, τ_w. The experimental system was able to produce the suction and blowing phenomena, but the control system was not able to deliver these counteracting flows effectively to reduce the overall skin friction drag.

7 FLUID DRAG REDUCTION PHYSICS AND APPLICATION CHALLENGES

It would be neither practical nor appropriate to investigate all of the possible FDR technologies for application to the high-speed ship. Preliminary engineering estimates indicate that the fast logistics ship total drag must be reduced by a factor of two (Genalis, 2000). Friction drag represents the greatest percentage of total drag, estimated to be approximately 70 percent of total drag. Assuming the residual 30 percent of total drag (form, wave, spray, etc.) already represents the optimum, and cannot be reduced, the friction drag must be reduced by a factor of four. This limits the FDR technologies that will be investigated to those that have demonstrated a reasonable chance of reducing friction drag by a factor of four, or by approximately 75 percent. The FDR technologies that come close to meeting this criterion is: microbubbles, polymers, surfactants, ventilation with super repellent coating, microfibers with polymer, and high viscosity fluid. Synergistic combinations of these technologies may yield significant friction drag reduction.

The FDR technology must not only reduce friction drag significantly, but also be capable of practical implementation on a full-scale ship, and be reliable under at-sea conditions, possibly including severe storms, and high speed maneuvering. FDR technologies that are "passive", or "always on" such as ventilation by super-cavitation would be the most preferable. Technologies where the drag reduction could be initiated with limited auxiliary equipment and a readily available (and low mass) "feed stock", such as microbubbles or blower induced ventilation, would be the next-most preferable technology. Technologies that require exotic auxiliary equipment and/or a significant quantity of "feed stock" to be carried by the ship, such as polymers or surfactants, would be the least preferable. This criterion effectively eliminates the fiber-polymer technology, due to practical considerations, and may ultimately eliminate polymers, surfactants and high viscosity fluid.

Improving Our Understanding of Turbulence Physics and FDR Technology: We have reviewed the role of drag with respect to ship design, identified the mechanisms of turbulence that contribute to friction drag specifically, noted the accomplishments of various drag reduction methodologies, and have selected a methodology worthy of further investigation. The fundamental physics and potential for practical application of this methodology must be analyzed in detail. Specifically, the following questions need to be investigated:

- Given the various mechanisms of turbulence generation, which mechanism(s) in particular can we most "practically" affect in order to reduce friction drag?
- How and why does a FDR technology "work" (understanding fundamental physics)? If it doesn't "work", why not?
- How effective is the FDR technology at high (full-scale, operational) speed?
- How effective is the FDR technology around complex shapes with an adverse pressure gradient?
- How effective is the FDR technology in salt (sea) water?

Applying FDR Technology to Large High-Speed Ships: The FDR technology may work well in the laboratory, and it may be possible to practically outfit a hull with the technology, but it may just not work when scaled up, and subject to the harsh environment of the open ocean. We must better understand how the FDR technology will behave under these conditions, specifically:

- What is the high-speed fluid flow around complex hull forms without FDR?
- How does the high-speed flow around a complex hull form affect the effectiveness of a FDR technology?
- How do we scale the subsequent laboratory results for speed and size?
- How effective is the FDR technology given unsteady pressure gradients and/or unsteady flow conditions during ship steady steaming and maneuvering (and how does the ship respond given unsteady FDR technology effectiveness)?
- How effective is the FDR technology given manufacturing imperfections over the hull surface, and hull biofouling?

Proposed Methodology for High-Speed Ship Testing: The following strategy is proposed to better understand the fundamental physics of turbulence and various, FDR technologies and how these FDR technologies may be scaled and applied to dynamic, "real world" situations. We need to conduct experiments to better determine turbulence and FDR technology physics fundamentals, at fluid flow speeds up to full-scale speed (38 m/s), for the following test configurations:

- Flat plate (no pressure gradient)
- Smooth and roughened surface
- Rotate plate orientation axially if the FDR is gravity dependent
- Foil plate (two dimensional pressure gradient) with similar tests as the flat plate
- Body of revolution: pipe (no pressure gradient)
- Body of revolution: axisymmetric body (quasi three-dimensional pressure gradient)
- Model ship half-body (three dimensional pressure gradient)

These experiments need to be performed in a pressurized facility to prevent unwanted cavitation at the higher test speeds. Eventually, we will want to know the effects of sheet cavitation and unsteady flow upon the effectiveness of the FDR technology, however, the initial experiments need to remain cavitation free in order to better isolate, and observe, the fundament physics. Several of these experiments should be performed using fresh and salt water, to determine the effect of salt water on the FDR technology (such as persistence). Details of the test equipment and instrumentation required are described by Ceccio (2002).

In order to take into account the free surface effects (unsteady fluid velocity, unsteady pressure gradient, and sheet cavitation), we need to conduct towing tank experiments at speeds up to full-scale speed (38 m/s) for the flat plate and foil, with and without the FDR technology applied.

By utilizing several sizes of test platform, and varying fluid flow speed over a broad range of speeds, we may be able to develop some basic scaling laws that could be combined with traditional scale model tests to provide a reasonable estimate for full-scale ship total drag.

Traditional model tests must be performed in a towing tank with the high-speed ship hull form, to provide basic ship resistance and seakeeping data. Modeling the extremely high volumetric flow rate water jets expected to propel the ship will be a non-trivial exercise. Cavitation number does not scale with model ship speed, via F-scaling, due to atmospheric pressure not being reduced commensurate with model scale. For most conventional ships and models, this is not an issue, due to the relatively high cavitation number for the model and full-scale ship. However, since the full-scale high-speed ship is expected to be a very high speed, relatively shallow draft vessel, different scale pressures between the model and ship will have a significant effect upon modeling sheet cavitation, cavitation-ventilation (as a FDR technology), and water jet efficiency. Atmospheric pressure may be scaled for the model by utilizing a pressure controlled towing tank. MARIN (Maritime Research Institute Netherlands) has the only reduced-pressure towing tank in existence. It is not likely that it will be practical to apply the FDR technology to the scale model for testing. However, it will be important to determine the effect of a FDR technology upon the water jet efficiency.

8 FACILITIES REQUIRED TO ACCOMPLISH EXPERIMENTS

The experimental measurements that are required to study the fundamental fluid mechanic problems associated with the design of high-speed ships and submarines are very involved and will require special instrumentation and testing facilities. It is most likely that a single facility will not suffice for all the tests. In the design and construction of any experimental facility, compromises must be made and they only seem to be exaggerated in high-speed testing facilities. The first decision to be made is whether to move the model or the have the fluid moving past a stationary model. Each technique has its advantages and disadvantages.

Moving models, such as in a towing tank, require an extremely long facility in order to have a reasonable testing time at very high speeds. The major advantages of moving the model are: the quiescent up-stream conditions are automatically satisfied; testing with a free surface is possible; and the power consumption to drive the towing carriage is reasonable. There are also many difficulties with a moving model arrangement. The biggest is probably the short testing window for steady conditions. Depending on the nature of the fluid transients at high Reynolds number, it is possible that steady state conditions are never reached. Regardless of how well the carriage is aligned,

there will always be vibration problems as a result of the high speed. This causes systemic errors in DPIV and LDA measurements since it is hard to distinguish between turbulence caused by the fluctuations of the flow field and apparent turbulence caused by the random vibrations of carriage and lasers. In addition, the forces associated with high Reynolds numbers are extremely large. This in turn will require a massive carriage to resist unwanted deflections. The massive carriage will inevitably make a significant free surface disturbance of its own that must be properly accounted for. Controlling the cavitation number in a towing tank type facility is difficult, if not impossible.

The other type of facility is to move the fluid past the model. If the facility is a continuous-circulation water channel, a massive amount of power is required. While the testing time in a circulating water channel is essentially unlimited, the up-stream conditions are not well defined and ambient turbulence might be a problem. An alternative moving-fluid facility is to have the fluid move impulsively past the model in a blow-down facility. This type of facility does not require the massive amounts of power to keep it running, but the steady state testing window is very short, probably less than a long towing tank. In either case, because the model is fixed, vibrations and deflections of the mounts will be minimized. DPIV and LDA measurements are easily accomplished through optical quality windows. Controlling the ambient pressure in the test section can control cavitation. A third type of moving-fluid facility is to use the fluid head behind a large dam to obtain a continuous high-speed flow. This approach has all the advantages of a circulating water channel, without the power losses. The cost of such a facility might be prohibitive, but it has been suggested to use the Detroit dam in Oregon.

A third option is to use full-scale field-testing. The big advantage of field-testing is that there are no questions about scale effects and realistic testing situations. However, controlling the quality of the data is usually a problem since many of the test variables are not under the control of the experimenter. In addition, full-scale testing is usually very expensive. All the problems of taking measurements in the towing tank are present and amplified in field-testing.

There are national facilities presently in operation that could conduct many of the desired tests. With relatively modest modifications, the existing facilities could probably do most of the desired tests. New facilities have the advantage of using the latest technology but they are much more expensive. The following is a list of the experimental facilities that are available in the United States that we believe could be used for high Reynolds number research. A more detailed review of each facility follows.

- The high-speed carriage at the Naval Surface-Ship Warfare Center, Carderock Division (NSWCCD). The David Taylor model basin high-speed facility was designed for speeds up to 51.4 m/s (100 knots), but present tests are limited to 30.9 m/s (60 knots) for models 1.2m up to 6.1m long.

- The 55-knot carriage at NSWCCD. The David Taylor model basin high-speed facility was designed for speeds up to 28.3 m/s (55 knots). Present tests confirm that the facility works well at full speed for models 1.2 m up to 6.1 m long.

- The Princeton/ONR HRTF uses air at pressures up to 3,500 psi as the working fluid, thereby decreasing the kinematic viscosity by over two orders of magnitude as compared to air at standard pressure. The main purpose of the facility is the study of the flow fields produced by submarine-type shapes up to length Reynolds number of 1.75×10^8. It has two test sections, each 2.44 m long with an internal diameter of 457 mm. Because the facility achieves its high Reynolds number from a change in kinematic viscosity and not from high velocity and large scale, it not of particular interest in studying drag reduction techniques on high-speed ships.

- The Navy's Large Cavitation Channel (LCC) located in Memphis, Tennessee. The LCC, operated by the Naval Surface Warfare Center, is the largest water tunnel in the world. It has a test section of 3 m x 3 m x 13 m and maximum velocity of 18.3 m/s. The flow speed in the test section could be increased to approximately 70kts by using a liner that reduces the cross sectional area (discussed further in the following section). The structure of the existing sections will have to be reinforced to accommodate the increased ambient pressure that is necessary for cavitation free operation.

- Applied Research Laboratory (ARL) at Pennsylvania State University. ARL has a variety of water tunnels with various size test sections. Of particular interest is the Garfield Thomas Water Tunnel. It has a 48inch-diameter test section and a maximum speed of 18.3 m/s.

- The Detroit Dam on the North Santiam River in Oregon is another possibility. The Detroit dam has a by-pass that could be use to direct water into a high-speed test facility. The large head of water behind the dam would be converted to velocity head by a nozzle leading to the test section.

- The Navy vessel *Athena. Athena I & II*, have seen extensive service in the development of high-speed towed sensors, airborne mine countermeasures, communication systems, and full-scale validations of model predictions for propeller wake surveys and propeller stress studies.

Large Cavitation Channel (LCC)

The Large Cavitation Channel (LCC) is one of the world's largest and most technically advanced water tunnel facilities. Operational in Memphis, Tennessee, USA since 1991, the LCC was designed as a variable pressure recirculating cavitation tunnel with a very low acoustic background level. The LCC provides significant cost savings for testing large-scale models of advanced ship and submarine system designs and full-scale torpedoes in a controlled environment. The LCC employs advanced hydro-acoustic silencing techniques for reducing acoustic reverberation introduced by the water flow of the tunnel. Commercial uses of this facility include maritime shipping industry applications.

Overall length	73 meters
Overall width	20 meters
Test section size	13 meters long x 3 meter cross section
Test section contraction ratio	6:1
Test section fluid velocity	2.6 – 18.0 meter/second
Pressure	3.5 – 414 kPa
Air content	10% - 100%

Table 2: LCC critical dimensions

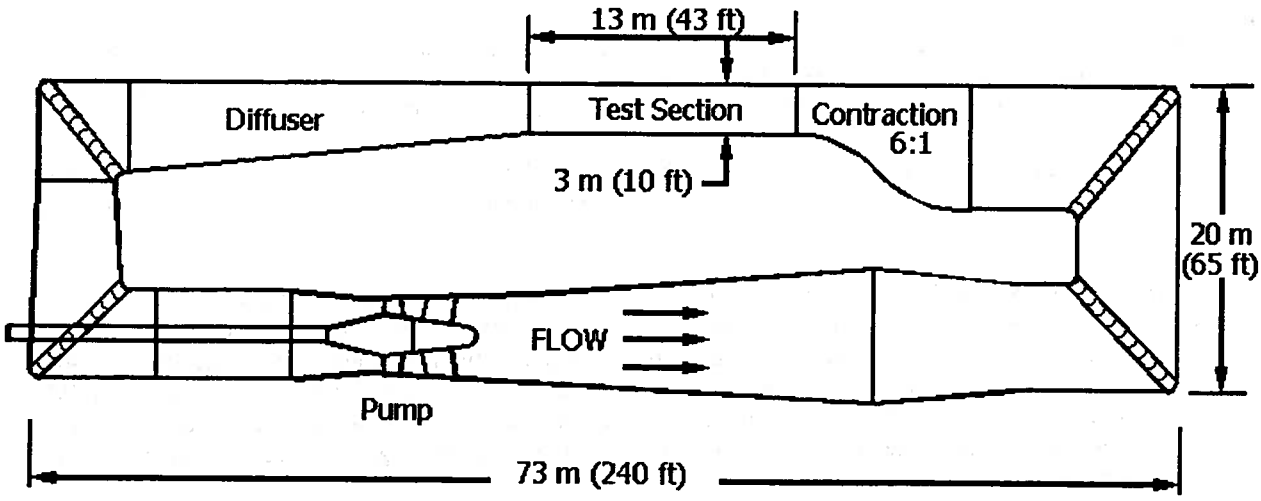

Figure 8: Side view of the William B. Morgan Large Cavitation Channel

The University of Michigan and its subcontractors have completed an initial design of a high-speed friction drag reduction experiment for implementation in the William B. Morgan Large Cavitation Channel (LCC) under support from the Office of Naval Research (Ceccio, *et al.*, 2002). Ceccio (2002) is meant to satisfy the reporting requirement of the first phase of the project. The three main elements of the friction drag reduction experiment have been developed, along with preliminary budget estimates for each element:

Modification of the LCC

The LCC typically operates at system pressures below atmospheric in order to evaluate the affect of cavitation on various test objects. The shell of the LCC is reinforced to handle the added stress due to the differential pressure. The LCC can also be pressurized to operate at pressures above one atmosphere in order to assist in suppressing cavitation on test objects. The global cavitation number is defined as $\sigma_{global} = (P-P_v)/(\frac{1}{2}\rho U^2)$, where U is the fluid free stream velocity, ρ is the fluid density, P_v is the vapor pressure of the fluid, and P is the free stream pressure of the system. For example, a 25-knot (12.86 m/s) ship would have a minimum global cavitation number of $\sigma_{global} = (1.013 \cdot 10^5 \text{ Pa} - 0.023 \cdot 10^5 \text{ Pa})/[\frac{1}{2} \cdot (1025 \text{ kg/m}^3) \cdot (12.86 \text{ m/s})^2] = 1.2$. The effect of hydrostatic pressure below the free surface would increase this value. Slower vessels will have an even higher σ_{global}. While the global cavitation number may be relatively large (greater than 1.0), local effects on the test object can have a much lower local cavitation number, σ_{local}, due to high local fluid velocity and low local pressure. Thus, cavitation can still occur on object with a complicated geometry with an adverse pressure gradient (such as a propeller) even though the global cavitation number is relatively high. However, a higher global cavitation number helps improve the odds that local cavitation effects can be minimized or eliminated. For the initial FDR tests on the test plate, we desire cavitation-free conditions in order to identify the effect of the FDR technology alone. Subsequent tests may include the effect of cavitation to observe how cavitation affects the FDR technology.

In order to achieve the required maximum test flow speeds and pressures, a liner could be implemented in the test section of the LCC that will reduce the cross sectional area of the test section to 3 m x 2.2 m. To achieve test section speeds up to 35 m/s, the electric motor of the LCC will be replaced. To achieve a test-section cavitation number of $\sigma_{global} = 0.75$ at 35 m/s (the estimated minimum σ_{global} required, and the maximum likely to be obtained), the ambient pressure in the test section will have to be raised to 470 kPa. At this pressure, the outer shell of the LCC will be stiffened in some high-stress areas. The impeller, stator, bearing, and shafting system do not require significant modification. A new pressure control system will be implemented to support large-scale air or water injection into the LCC. The remaining auxiliary systems do not require significant modification. The estimated cost of the LCC modification is discussed in Ceccio, *et al.* (2004).

The Detroit River Dam

The Army Corp of Engineering personnel at the DRD provided the following specifications for the dam:

General Specifications:	
Drainage area	438 square miles
Pool elevations (feet above mean sea level)	
Minimum power pool	1425 ft
Minimum flood control pool	1450 ft
Maximum conservation pool	1569 ft
Maximum full pool	1425 ft
Reservoir Specifications:	
Maximum pool	472,600 acre-feet
Maximum conservation pool	436,000 acre-feet
Minimum flood control pool	154,400 acre-feet
Minimum power pool	115,000 acre-feet
Dam Specifications:	
Type	Straight concrete gravity
Crest length	1457 ft
Crest elevation	1579 ft
Crest width	26.5 ft
Maximum height	450 ft
Freeboard (above max. pool)	5 ft
Spillway Specifications:	
Type	Concrete gravity, gate controlled
Design Discharge	176,000 cubic ft/second
Crest length	294.5 ft
Crest elevation	1541 ft
Number, size and type gates	Six Radial, 45 ft x 48 ft
Outlet Works:	
Type	Conduit through dam
Emergency gates	Four Fixed Wheel, 5 ft 8 inch x 10 ft
Regulating gates	Four Fixed Wheel, 5 ft 8 inch x 10 ft
Power-Plant:	
Penstocks	Two 15 ft diameter steel
Power units	2 Francis Turbines
Installed capacity	100,000 Kilowatts

Table 3: Detroit River Dam dimensions and operating parameters

The High Velocity Test Conduit and Test Flume

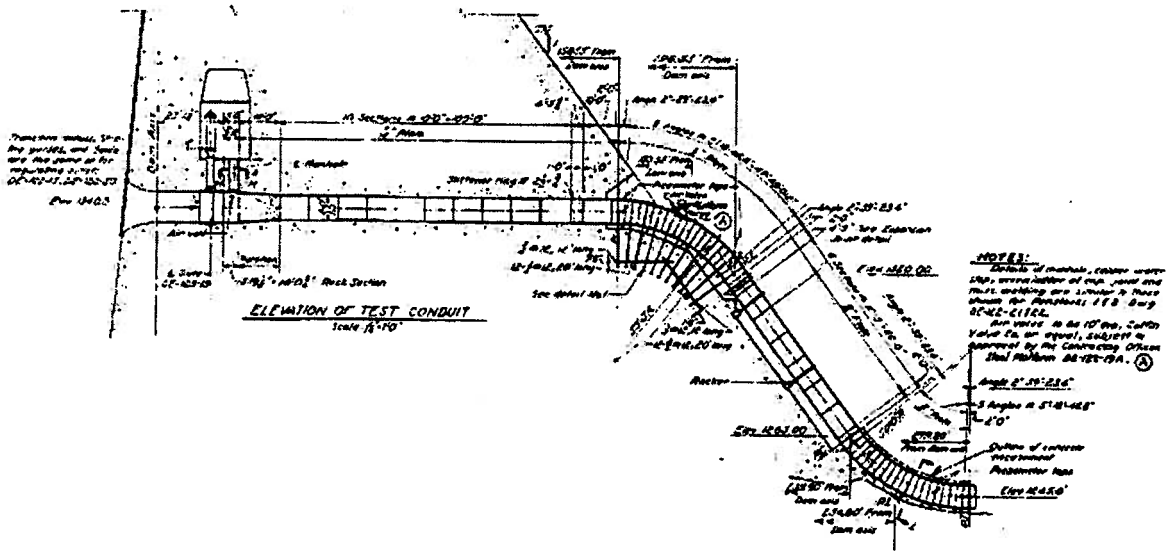

Figure 9: Cross section of the Detroit River Dam

cavitation of the test model and test section walls. The above considerations are the result of the Bernoulli analysis and are independent of the flow rate through the test section (i.e. the test section cross sectional area). Speeds in excess of ~ 32 m/s (107 ft/s) can be achieved if the models are allowed to supercavitate.

Figure 10: Test section velocity and pressure for case of full pool with total head ~ 99 m (325 ft) and flood control pool with total head ~ 63 m (207 ft)

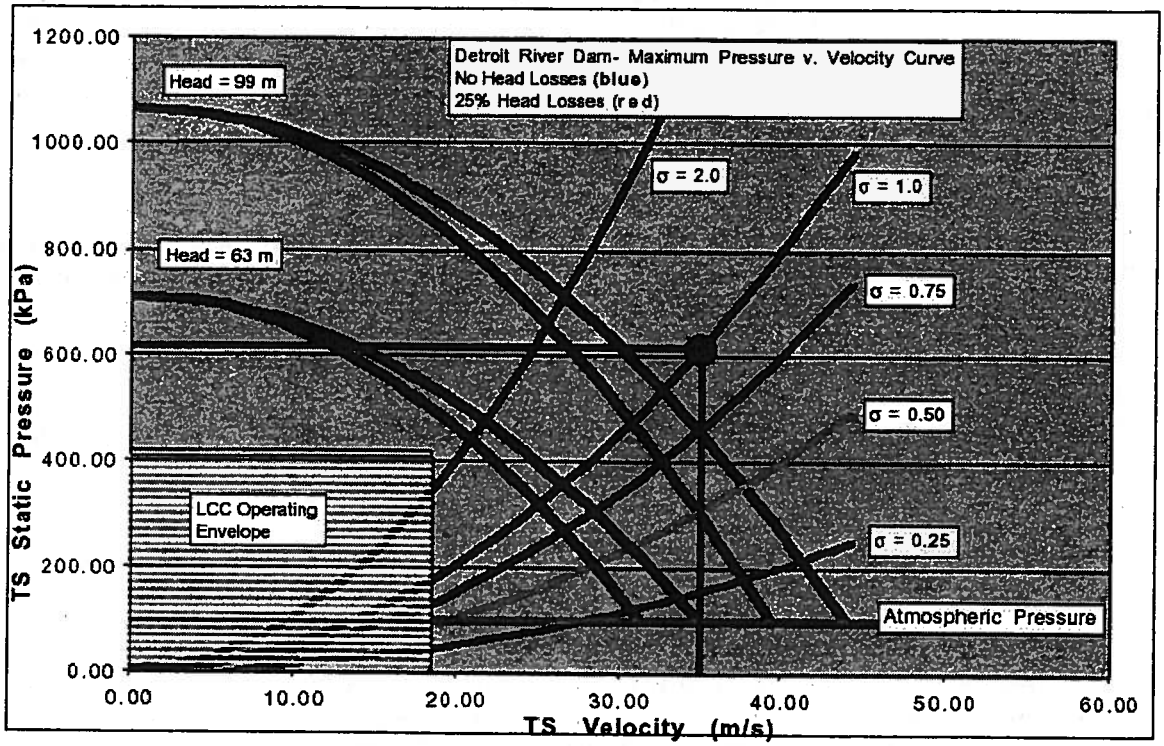

The amount of water that flows across the dam varies during different periods of the year. If the test flume operates only during times that the DRD spillway is in use, then the operation of the hydroelectric plant at the DRD will not be significantly effected. However, the yearly number of days that the spillway is in use is low, and the timing and duration of the spillway usage is hard to predict. If the test flume were to be used during the remaining periods of high pool, the flux of water across the dam would need to be divided between the test-flume and the hydroelectric plant. If the daily flow through the test flume is small compared to that of the power plant, the impact of flume operation on power generation will be minimal. However, if a large diameter test flume is constructed, there could be significant competition with the power plant for the water flow. Since the spillway is in use only a handful of days during the year, we will consider operation during periods when the outflows are principally through the generators.

Flows up to 300,000 CFM will pass through the hydroelectric plant. Flows in excess of 300,000 will require water to pass through the DRD spillway. The largest flow rate achievable through the DRD test-flume penstock will occur if the test-section cross-section is on the order of the penstock cross section, which is 2.4 m (8 ft) in diameter. If the test section velocity is 35 m/s (110 ft/s), the flux of water through the penstock would be approximately 350,000 CFM. The flux of water through through a large test-flume will be on the order of the flows through the generators. Since the total flow of water through the dam is carefully controlled, it is possible that operation of the test-flume will lead to a reduction in the production of electricity at the DRD. It is not clear, however, that the operators of the hydroelectric generating plant would permit significant interruption of their power generation. A balance must then be made between the size of the test flume, and the amount of time it is expected to operate.

Significant portions of the existing DRD test flume will need to be replaced, possibly including the existing penstock. The current test flume sits on the right bank of the tailrace, on a ledge next to a rock face. A new test section and accompanying platforms and housing would be confined to this narrow space between a rock ledge and the bank of the tailrace. Otherwise, the test section would need to be moved significantly downstream of the dam. A

narrow bridge connects the main road to the site of the test section. All of the construction equipment and pieces of the test section would need to pass over this narrow bridge, leading to practical difficulties with construction and operation of the test site. Additionally, high-tension lines will make crane-work difficult. There are few engineering facilities at the DRD. Engineering facilities at the DRD would have to be constructed around the test flume and nearby for personnel, storage, model preparation, etc.

The test facility would take in ambient lake water and discharge it. It is often necessary to control the inlet water quality for testing. Factors such as the free and dissolved gas content, the water temperature, and the level or particulates and other foreign matter would be difficult to control. More importantly, it is possible that dyes, particles, polymers or surfactants may be injected into the flow stream during friction drag reduction testing. While these substances may be considered benign, it is not clear that operators of the test facility can gain permission to discharge these substances into the environment without treatment.

Summary

The current test flume of the DRD is not operable, but it is possible to construct a new test facility at the DRD. Such a blow-down facility would be best suited for the study of super-cavitating and ventilated test objects. The likely characteristics and challenges associated with the construction and operation of such a new facility would be the following:

- The current test flume must be replaced.
- If the test objects super-cavitate, it is likely that flows of up to ~40 m/s can be achieved during periods at full pool, and up to ~30 m/s at flood control pool.
- If the test objects are not permitted to cavitate, then flows of up to ~30 m/s can be achieved during periods at full pool, and up to ~25 m/s at flood control pool.
- If the current penstock is used, the circular cross sectional area of the new test flume would be approximately 0.75 m (2.5 ft) in diameter for high-speed operation.
- The period during the year when conditions for high speed testing are optimal may be significantly limited (e.g. full pool and high discharges).
- Increased test sectional areas would likely require a new penstock, dam penetration, and upstream valves.
- The potential energy cost of operating such a test flume with a 2 to 3 ft diameter would be ~$600 per hour (assuming $40 MW-hour cost). The cost increases as the square of the test section diameter. At high flow rates, the daily duration of testing may be limited by the needs of power generation. These costs would not be incurred during the (infrequent) days when the DRD spillway is in use.
- There may be significant logistical difficulties for the construction and operation of the new test facility.
- There may be significant environmental issues regarding the discharge of polymer or other chemical additives via the untreated flow of the test flume. In addition, the discharge of water may be limited due to environmental constraints (e.g. restraints on the pool level and downstream flow rates).

Carderock Division Naval Surface Warfare Center (NSWC/CD) High-Speed Basin Carriage #6

Towing Basins can be used for traditional Froude-scaled ship model resistance, self-propulsion and flow measurement experiments. The towing carriages may be used for a variety of unusual experiments, including towing of fishing nets, calibration of current meters, control station for remotely operated vehicles, and assessing stability of towed bodies. Commercial uses for this facility include maritime shipping industry, fishing industry, oceanographic engineering, and pleasure craft industry applications.

The NSWCCD High-Speed Basin is comprised of two adjoining sections: a deep-water section and a shallow water section. Wave making capability exists in this basin, and there are three large underwater viewing windows at different elevations, which are set into the wall about mid-length. This indoor rectangular high speed basin with a total length of 904 m (2968 ft) comprises two adjoining sections:

- Deep water - 4.9 m (16 ft) deep, approx. 514 m (1687 ft) long and 6.4 m (21 ft) wide
- Shallow water - 3 m (10 ft) deep, approx. 356 m (1169 ft) long and 6.4 m (21 ft) wide

The U.S. Navy envisioned the need for a high speed towing test facility capable of operating at speeds up to 100 knots as long ago as the late 1960's. The initial design investigation centered on lengthening an existing towing basin at the NSWCCD facility. The basin would need to be longer in order to allow more time and distance for the

carriage to get up to the higher test speeds, and still allow a reasonable period of time at the higher test speed for data collection. Cost analysis of various engineering designs indicated a very high cost to lengthen the towing basin facility. Alternative designs based upon very high acceleration of a new carriage on the existing towing basin were investigated.

A design utilizing linear induction motors on a completely new carriage was installed and tested (designated as Carriage #6) during the mid 1970's through 1980, sharing the same towing basin and rails as Carriage #3 and Carriage #5. The mechanical and motor systems passed inspection and testing, however, there were significant problems with the electronic control, power supply conditioning, and data communication systems. The U.S. Navy ceased attempting to get Carriage #6 to an operational status in 1980, and all systems remain as they were at that time.

		2-Motor Drive	4-Motor Drive
Tank width	31 feet		
Tank depth	10 feet		
Carriage weight	61,000 pounds		
Carriage material	Aluminum		
Maximum tractive force	40,000 pounds		
Maximum drag load	22,000 pounds		
Maximum lift load	30,000 pounds		
Maximum side load	15,000 pounds		
Maximum speed		75+ knots	100 knots
Maximum acceleration		0.61 g	1.12 g
Test distance/time, given:	15k pounds drag at 70 knots	787 ft / 7 seconds	1507 ft / 13 seconds
	15k pounds drag at 80 knots	419 ft / 3 seconds	1359 ft / 10 seconds
	22k pounds drag at 70 knots	226 ft / 2 seconds	1446 ft / 12 seconds
	22k pounds drag at 80 knots	N/A	1279 ft / 9 seconds
	22k pounds drag at 100 knots	N/A	879 ft / 5 seconds

Table 4: NSWCCD Carriage #6 critical dimensions and operational parameters

A recent engineering study concluded that the following sub-systems would have to be replaced in order to put Carriage #6 into operation: variable frequency power conditioning system, control system, data communications system, hydraulic brake system. In addition, the linear induction motor electric rail system and the towing tank carriage wheel rails will need to be refurbished.

The costs associated with getting Carriage #6 outfitted to perform at 75 knots (2 motors) is estimated to be $4.1 million. The costs associated with getting Carriage #6 outfitted to perform at 100 knots (4 motors) is estimated to be $7.2 million. The time required to refurbish the carriage would be approximately 3 years.

Full-Scale Engineering Facilities

A large-scale at-sea test platform can provide critical operational testing that can not be modeled in a laboratory setting. FDR technologies that perform well under controlled laboratory conditions may perform well only intermittently, or not at all, in the complex environment of a sea-going vessel. The at-sea test platform can permit large-scale field testing, without incurring the enormous risk of completely outfitting an active naval combatant with an unproven technology. However, these test platforms have proven to be poor "laboratories"; meaning that determining exactly why a tested technology succeeds or fails can be difficult, if not impossible, due to having so many uncontrolled variables at sea. Despite the scientific deficiencies, there is likely a cost benefit to having a large-scale at-sea test platform to conduct implementation tests of FDR technologies.

R/V Athena

Athena I & II, have seen extensive service in the development of high speed towed sensors, airborne mine countermeasures, communication systems, and full-scale validations of model predictions for propeller wake surveys and propeller stress studies.

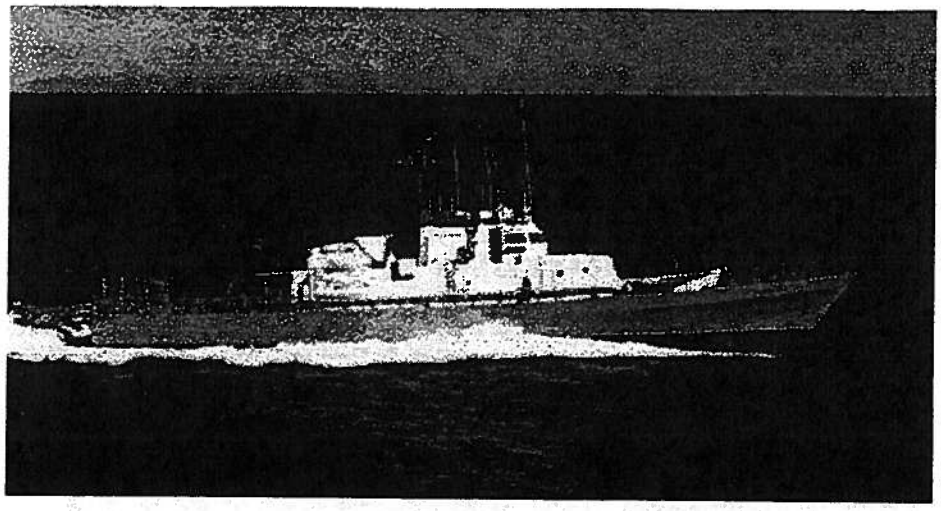

Figure 11: R/V *Athena*

Athena is a converted PG-84 Asheville-class patrol gunboat. Built for the U.S. Navy in 1969 at Tacoma Boat as *USS Chehalis* (PG-94), she was converted to a high-speed research vessel in 1976. The hull and structural framework are aluminum alloy, and the superstructure is fiberglass over an aluminum framework. Since *Athena* was built as a high-speed patrol gunboat, she was engineered to be as lightweight as possible and constructed under high standards of quality assurance.

Because of her combination of diesel or gas turbine propulsion, *Athena* is well suited for low- or high-speed operations. To enhance *Athena*'s capability in taking high-speed acoustic data, she can be fitted with a compound air masker system (CAM), which greatly reduces the ship's radiated noise. She has been modified extensively as a Research Vessel to include: laboratory space with a dedicated power source, deck crane, and A-Frame. A variety of towing winches and handling equipment is available as required.

Specifications:

Length Overall	165 feet
Extreme Beam	24 feet
Draft	10.5 feet
Propulsion	Twin screw, driven by two Cummins VT12-875-M diesel engines rated at 725 h.p. each. For high speed one GE LM 1500 gas turbine drives both propellers through a first, and two secondary gearboxes.
Speed	13 knots on diesel, 35 knots on turbine
Fuel Consumption	90 gallons per hour at 13 knots 500 gallons per hour at 20 knots 850 gallons per hour at 30 knots 1,000 gallons per hour at 35 knots
Range	2300 n.m. cruising at 13 knots
Electrical	Two 100 kW ship service generators. One 60 kW lab generator
Accommodations	Berthing for 28, (10 crew, 18 scientists)
Laboratory Space	366 sq. ft. of air conditioned lab space is available. Power is provided by a dedicated 60 kW generator via regulating transformers for clean, precise power.
Clear Deck Space	850 sq. ft. on the aft deck
Nav/Communication	Radar, GPS, Sat-Nav, LORAN, Fathometer, Gyro- compass, Knotmeter, SSB radio, VHF, UHF

Table 5: Athena critical dimensions and operating parameters

X-Craft

The X-Craft transformational program is a high-speed, 240-foot aluminum catamaran consisting of advanced hull geometry, designed to give the craft speeds of 50 knots or more. Initially, it will be used by ONR for purposes of hydrodynamic experimentation and as a test bed for Hull, Mechanical, and Electrical (HME) concepts for the Navy's new class of warship, Littoral Combat Ship (LCS).

The X-Craft's deck will have two helicopter landing spots capable of handling a variety of aircraft up to the size of the H-60-series helicopter. With a design displacement of approximately 1,100 long tons, the X-Craft will be self-deployable and of flexible design for spiral technology insertion.

A Combined Gas Turbine or Diesel (CODOG) propulsion plant will propel the X-Craft to speeds of 50 knots or more. The vessel's Mission Module Bay will be capable of fully supporting simultaneously two or three mission packages designed for the Navy's littoral combat support. In February 2003, the Office of Naval Research awarded Titan a $59.9 million contract to develop and build the Navy's X-Craft.

The X-Craft may prove to be an effective field test platform for FDR technologies at full scale and very high Reynolds number, when it enters service.

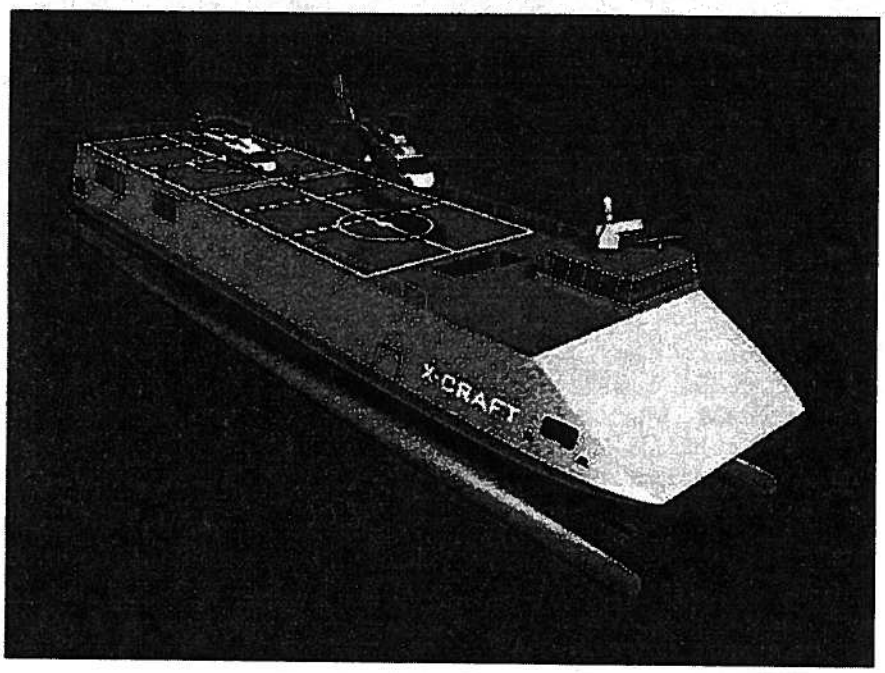

Figure 12: Conceptual model of the *X-Craft*

9 Conclusion and Recommendations

High speed surface and submerged vessels that displace several thousand tons or more, capable of operating at speeds in excess of 50 knots, and spanning an entire ocean without refueling will need to utilize a FDR technology in order to be practical to design and operate cost effectively. Ships capable of meeting one or two of the previously listed criteria already exist. Designing a ship that meets all three criteria without the benefit of FDR technology would seriously challenge what is considered possible by the current state-of-the-art design process. The FDR technology itself will also have to be practical to implement and utilize. The ship and FDR auxiliary equipment must be capable of: carrying or generating sufficient quantities of the FDR material without undue impact to the payload capacity of the vessel; the auxiliary equipment must be reliable, with appropriate redundant systems; the system must be operable and maintained, at sea and in port, by professional sailors with a reasonable amount of specialized technical training; the FDR deployment mechanism (e.g. nozzles) that is subject to the high hydrodynamic forces and marine fouling must remain effective, even though some degradation of the mechanism may occur between maintenance and cleaning events.

Numerical and experimental analysis of turbulent flows at the smallest observable scales has yielded significantly new insight into the mechanisms of turbulence, and the behavior of the major structures within the boundary layer. The "streak-liftup-hairpin-burst-sweep" cycle of turbulence regeneration provides a conceptual model around which we may build a strategy to affect the control of turbulence. One or more of these events within the cycle of turbulence regeneration must be controlled in order to reduce total friction drag. The interaction between each of these mechanisms has only recently been observed and conceptualized through advanced numerical and experimental means, and the model may undergo further refinement as the investigation continues. Additional investigation into the mechanisms of turbulence is critical to finding the FDR technology that would most appropriately match the needs of a high-speed ocean-going vessel. For some of the FDR technologies reviewed in this report, we may deduce which turbulence regeneration mechanism is being modified/suppressed (e.g. high viscosity fluid may function by suppressing the burst effect), however, for the vast majority of FDR technologies, we really don't understand what mechanism they use to affect the turbulence regeneration cycle. Understanding the fundamental physics of the FDR technology is prudent, prior to making an attempt to implement the FDR technology onto a full-scale, operational vessel, if there is to be a chance of success within a reasonable period of time. Several attempts to "shotgun" a solution from promising, but basic, laboratory results to deployment of a prototype system onto a full-scale ship have met with disappointment.

The summary of FDR technologies reviewed in this paper demonstrates that a great deal of effort has gone into better understanding the effects, and to some extent, the fundamental physics, of these technologies. A few of the FDR technologies, such as microbubbles, surfactants and polymers, have demonstrated friction drag reduction capabilities near the target value of 70 percent. However, all of these tests occurred under laboratory conditions at relatively slow fluid velocities. As previously mentioned, some of these FDR technologies have been tested or used on full-scale systems, with poor results. None of the FDR technologies have been tested at the speed, or complex pressure gradient, required for a high-speed logistics ship, or underwater missile, etc. Scaling laws for the various FDR technologies are unknown, and indeed, may be too complicated to be practical. Hence, the need to test the FDR technology at the full-scale high speed conditions to better understand its interaction with the mechanisms of turbulence.

Initial testing of a FDR technology will be very "basic" (testing at high speed on a flat, cavitation-free plate in fresh water), focusing on understanding the fundamental physics of the technology, and the mechanisms of turbulence. The outcome from these tests may yield some insight that would permit some improvement of the FDR technology itself, and/or require an improvement of the test methods or instrumentation. An iterative FDR improvement cycle, between high-speed, full-scale tests, using advanced numerical methods or slower, small-scale testing, may be implemented simultaneously to investigate a FDR improvement. Subsequent tests on complex shapes, including various pressure gradients, will be necessary to determine how the FDR technology will behave in complex flows (evaluating the effect of persistence, etc.).

No test facility currently exists that meets all of the requirements to investigate the mechanisms of turbulence or test the FDR technologies at the necessary fluid speeds, pressure gradients, and length scales. To construct a new facility dedicated to this purpose may be prohibitively expensive in both time and capital. A few of the existing facilities come close to meeting some of the testing requirements, and could be modified into acceptable test facilities, even if not perfect, if some engineering improvements were made. As the discussion in this paper shows, the LCC facility and the Detroit River Dam site represent the kind of facility that is appropriate for the initial phase of the testing. A separate program has already been initiated to begin making several small improvements to the LCC to support the first phase of FDR testing. A phased-approach to making the engineering improvements to

the LCC, in conjunction with the FDR testing process, makes the best use of time and capital. Minor improvements to the LCC system for little capital will allow initial FDR testing to begin with capabilities far beyond what has previously been documented. The results of these initial tests may help point the direction of subsequent testing, possibly in ways that were previously unforeseen. Subsequent engineering improvements can be developed while FDR testing continues. Therefore, the most efficient and prudent solution is to make the best use of the LCC test facility, making incremental improvements as FDR testing evolves.

The full battery of FDR tests will require high speed, submerged non-cavitating and cavitating flow tests; high speed free surface tests; and full-scale open water tests. In keeping with the prudent but efficient approach toward testing, the Carderock High Speed Carriage #6 should be considered the facility of choice for the free surface tests, after the appropriate engineering improvements are made. However, making improvements to Carriage #6 should wait until satisfactory progress has been made during the initial stages of testing at the LCC to warrant the capital expenditure.

The final phase of testing will be on a full-scale, high-speed, open water test platform. The FDR will have to prove its effectiveness in seawater, in a complex flow with a dynamic, complex pressure gradient, subject to a hull with imperfections from construction and marine fouling. Some of these effects may be simulated individually in the high-speed channel or towing tank, but there is no substitute for evaluating the combined effect on FDR performance. The test platform will also be the field laboratory for developing a robust and effective FDR delivery system. Having a reliable, maintainable, and cost effective delivery system is just as important as having an effective FDR technology itself.

References

Adrian, R. J. & S. Balachandar (1998) Vortex Packets and the Structure of Wall Turbulence, *Proc. Int'l. Symp. on Seawater Drag Reduction*, pp. 33–38

Akhavan, R., W. J. Jung & N. Mangiavacchi (1992) Suppression of Turbulence in Wall-Bounded Flows by High-Frequency Spanwise Oscillations, *Physics of Fluids A*, **4**(8):1605–7

Alfredsson, P. H. & A. V. Johansson (1984) On the Detection of Turbulence-Generating Events, *J. of Fluid Mechanics*, **139**:325-45

Anderson, G. W., J. J. Rohr & S. D. Stanley (1993) The Combined Drag Effects of Riblets and Polymers in Pipe Flow, *J. Fluids Engineering*, **115**:213–20.

Barlow, J. B., W. H. Rae & A. Pope (1999) *Low-Speed Wind Tunnel Testing*, Interscience, 728 p.

Baron, A. & Quadrio, M. (1996) Turbulent Drag Reduction by Spanwise Wall Oscillations, *Applied Scientific Research*, **55**:311–26

Beys, P. M. (1963) Series 63 Round Bottom Boats, DL Report 949

Bogdevich, V. G., L. I. Maltzev & A. G. Maluga (1998) Optimization of the Distributed Gas Injection into a Turbulent Boundary Layer for the Drag Reduction, , *Proc. Int'l. Symp. on Seawater Drag Reduction*, pp. 327-330

Broadbent, C. & Kennell, C. (2001) Monohull, Catamaran, Trimaran, and SES High Speed Sea Lift Vessels, NSWCCD, 11 p.

Carpenter, P. W. (1998) Current Status of the Use of Wall Compliance for Laminar-Flow Control, *Experimental Thermal and Fluid Science*, **16**:133–40

Ceccio, S. L., R. Beck, D. Dowling, M. Perlin (2002) Design of a High-Speed Friction Drag Reduction Experiment Using the William B. Morgan Large Cavitation Channel, Office of Naval Research, Report Number 02-014

Choi, H., P. Moin & J. Kim (1994) Active Turbulence Control for Drag Reduction in Wall-Bounded Flows, *J. Fluid Mechanics*, **262**:75–110

Choi, K. S., X. Yang, B. R. Clayton, E. J. Glover, M. Altar, B. N. Semenov, V. M. Kulik (1997) Turbulent Drag Reduction Using Compliant Surfaces, *Proc. Royal Soc. London*, **453**:2229–40

Choi, K.-S. & B. Clayton (1998) Mechanisms of Turbulent Drag Reduction with Wall Oscillation, *Proc. Int'l. Symp. on Seawater Drag Reduction*, pp. 229–35

Clement, E. P. & D. L. Blount (1963) Resistance Tests of a Systematic Series of Planing Hull Forms, SNAME

Coleman, G. N., J. Kim & A.-T. Le (1996) A Numerical Study of Three-Dimensional Wall-Bounded Flows, *Int'l. J. Heat and Fluid Flow*, **17**:333–42

DeGraaff, D. B. & J. K. Eaton (2000) Reynolds-Number Scaling of the Flat-Plate Turbulent Boundary Layer, *J. Fluid Mech.*, **422**:319-46

Dimotakis, P., P. Diamond, F. Dyson, D. Hammer, J. Katz & D. Nelson (2000) Turbulent Boundary-Layer Drag Reduction (slide presentation), Jason DARPA study, JSR-00-135

Du, Y., C. H. Crawford & G. E. Karniadakis (1998) Lorentz Force Modeling in EMHD Turbulence Control: DNS Studies, *Proc. Int'l. Symp. on Seawater Drag Reduction*, pp. 407-12

Fan, X., & G> L. Brown (1998) Experiments on Turbulent Channel Flow with Electromagnetic Turbulence Control, *Proc. Int'l. Symp. on Seawater Drag Reduction*, pp. 369-71

Ferziger, J. H. (1996) *Computational Methods for Fluid Dynamics*, Springer-Verlag New York, 423 p.

Fukuda, K., J. Tokunaga, T. Nobunaga, T. Nakatani, T. Iwasaki & Y. Kunitake (2000) Frictional Drag Reduction With Air Lubricant Over a Super Water Repellent Surface, *J. Marine Science and Tech.*, **5**:123–30

Gad-el-Hak, M. (1998) Compliant Coatings: The Simpler Alternative, *Proc. Int'l. Symp. Seawater Drag Reduction*, pp. 197–204

Genalis, P. (2000) Fast Logistics Ships (slide presentation), OUSD (AT&L)/Strategic and Tactical Systems/Naval Warfare, August 2000

Granville, P. S. (1958) The Frictional Resistance and Turbulent Boundary Layer of Rough Surfaces (Report 1024), David Taylor Model Basin Hydromechanics Laboratory, 45 p.

Guin, M. M., H. Kato & Y. Takahashi (1998) Experimental Evidence for a Link Between Microbubble Drag Reduction Phenomena and Periodically Excited Wall-Bounded Turbulent Flow, *Proc. Int'l. Symp. on Seawater Drag Reduction*, pp. 313-18

Hendrix, D., S. Percival & F. Noblesse (2001) Practical Hydrodynamic Optimization of a Monohull. *Trans. SNAME*, **109**:173–83

Holling, H. D. & N. Hubble (1974) Model Resistance Data of Series 65 Hull Forms Applicable to Hydrofoils and Planing Craft, NSRDC Report Number 4121

Holtrop, J. & G. G. J. Mennen (1982) An Approximate Power Prediction Method, *Int'l. Shipbuilding Progress*, Vol 29, No 335

Hoyt, J. W. (1998) Polymer Solution Effects on Turbulent Friction Mechanisms, *Proc. Int'l. Symp. on Seawater Drag Reduction*, pp. 1–5

ITTC (1957) *Proceedings of the 8th ITTC, Madrid, Spain*, Canal de Experiencias Hidrodinamicas, El Pardo, Madrid

Kato, H., Y. Fujii, H. Yamaguchi & M. Miyanaga (1993) Frictional Drag Reduction by Injecting High-Viscosity Fluid into Turbulent Boundary Layer, *J. Fluids Engineering*, **115**:206-12

Kato, H., M. Miyanaga, Y. Haramoto & M. M. Guin (1994) Frictional Drag Reduction by Injecting Bubbly Water into Turbulent Boundary Layer, FED Vol.190, Cavitation and Gas-Liquid Flow in Fluid Machinery and Devices, ASME 1994: 185-194

Kawaguchi, Y., T. Segawa, Z. Feng & P. Li (2002) Experimental Study on Drag-Reducing Channel Flow with Surfactant Additives–Spatial Structure of Turbulence Investigated by PIV System, *Int'l. J. Heat and Fluid Flow*, **23**:700–09

Kodama, Y. (1998) Effect of Microbubble Distribution on Skin Friction Reduction, *Proc. Int'l. Symp. on Seawater Drag Reduction*, pp. 331-34

Koskie, J. E. & W. Tiedermann (1991) Turbulence Structure and Drag Reduction in Adverse Pressure Gradient Boundary Layers (ONR Report PME-FM-91-3), School of Mechanical Engineering, Purdue University.

Krämer, M. O. (1960) The Dolphin's Secret, *New Scientist*, **7**:1118

Krämer, M. O. (1962) Boundary Layer Stabilization by Distributed Damping, *J. American Soc Naval Eng.*, **74**:341

Kuhn, J. (2002) The SHAPE Code: A Tool for Automated Hull Form Development. SAIC Technical Report SAIC-02/1004 Rev. A, 11 p.

Kundu, P. K. & I. M. Cohen (2002) *Fluid Mechanics*, Academic Press San Diego, 730 p.

Kulik, V. M. (1998) Drag Reduction Dynamics, *Proc. Int'l. Symp. on Seawater Drag Reduction*, pp. 299-301

Latorre R. (1997) Ship Hull Drag Reduction Using Bottom Air Injection, *Ocean Engineering*, **24**(2):161-75

Latorre, R. & V. V. Babenko (1998) Role of Bubble Injection Technique in Drag Reduction, *Proc. Int'l. Symp. on Seawater Drag Reduction*, pp. 319-321

Lu, B., X. Li, J. L. Zakin & Y. Talmon (1997) A Non-Viscoelastic Drag Reducing Cationic Surfactant System, *J. Non-Newtonian Fluid Mechanics*, **71**:59–72

Madavan, N. K., S. Deutsch & C. L. Merkle (1984) Reduction of Turbulent Skin Friction by Microbubbles, *Physics of Fluids*, **27**(2):356–63

Madavan, N. K., S. Deutsch & C. L. Merkle (1985) Measurements of Local Skin Friction in a Microbubble Modified Turbulent Boundary Layer, *J. Fluid Mechanics*, **156**:237-56

Maltzev, L. I. (1995) Jet Methods of Gas Injection into Fluid Boundary Layer for Drag Reduction, *Applied Scientific Research*, **54**:281–91

Mathieu, J. & J. Scott (2000) Introduction to turbulent Flow, Laboratoire de Mécanique des Fluides et d'Acoustique, Ecole Centrale de Lyon, France, Cambridge University Press.

Meinhart, C. D. & R. J. Adrian (1996) On the Existence of Uniform Momentum Zones in a Turbulent Boundary Layer, *Physics of Fluids* **7**:694–96

Meng, J. C. S. (1998) Engineering Insight of Near-Wall Microturbulence for Drag Reduction and Derivation of a Design Map for Sea Water Electromagnetic Turbulence Control, *Proc. Int'l. Symp. Seawater Drag Reduction*, pp. 359–67

Meng, J. C. S. & J. S. Uhlman, Jr. (1998) Microbubble Formation and Splitting in a Turbulent Boundary Layer for Turbulence Reduction, Naval Undersea Warfare Center, Newport, Rhode Island, 1998

Merkle, C. L. & S. Deutsch (1992) Microbubble Drag Reduction in Liquid Turbulent Boundary Layers, *Applied Mechanics Review*, Part 1, **45**(3):103–27

Metzner, A. (1977) Polymer Solution and Fiber Suspension Rheology and Their Relationship to Turbulent Drag Reduction, *Physics of Fluids*, Part II, **10**:S145–49

Mochizucki, S. & H. Osaka (1998) Drag Reduction with Submerged Ribs and Its Mechanism in a Turbulent Boundary Layer Over D-Type Roughness, *Proc. Int'l. Symp. on Seawater Drag Reduction*, pp. 121-26

Myska, J., J. L. Zakin & Z. Chara (1996) Viscoelasticity of a Surfactant and Its Drag Reducing Ability, *Applied Scientific Research*, **55**:297–310

NAVSEA DDS 051-1 (1984) Prediction of Smooth-Water Powering Performance for Surface-Displacement Ships, Naval Sea Systems Command

Oliver, D. R. & S. I. Bakhtiyarov (1983) Drag Reduction in Exceptionally Dilute Polymer Solutions, *J. Non-Newtonian Fluid Mechanics*, **12**:113–18.

O'Sullivan, P. L. & S. Biringen (1998) Fundamental Studies on Active Control of Large Scale Coherent Structures in Channel Turbulence, *Proc. Int'l. Symp. on Seawater Drag Reduction*, pp. 413–418

Philips, R. B., J. M. Castano & J. Stace (1998) Combined Polymer and Microbubble Drag Reduction, *Proc. Int'l. Symp. on Seawater Drag Reduction*, pp. 335-40

Prohaska, C. W. (1966) A Simple Method for the Evaluation of the Form Factor and Low Speed Wave Resistance, *Proc. 11th ITTC*

Ptasinski, P. K., F. T. M. Nieustadt, B. H. A. A. Van der Brule & M. A. Hulsen (2001) Experiments in Turbulent Pipe Flow with Polymer Additives at Maximum Drag Reduction, *Flow Turbulence and Combustion*, **66**:159–82

Ragab, S. A. (2003) Shape Optimization in Free Surface Potential Flow Using an Adjoint Formulation, NSWC/CD Report NSWCCD-50-TR–2003/033, viii+111 p.

Schultz, M. & G. Swain (1998) The Effect of Biofilms on Turbulent Boundary Layer Structure, *Proc. Int'l. Symp. on Seawater Drag Reduction*, pp. 175-81

Smagorinski, J. (1963) General Circulation Experiments with the Primitive Equations, Part I: The Basic Experiment, *Monthly Weather Rev.*, **91**:99-164

Smith, C. R. (1998) Vortex Development and Interactions in Turbulent Boundary Layers: Implications for Surface Drag Reduction, *Proc. Int'l. Symp. Seawater Drag Reduction*, 1998, pp. 39–46

SNAME Technical & Research Report R-18 (1975), Effects of Bottom Maintenance on Frictional Resistance of Ships, Society of Naval Architects and Marine Engineers, New York, 13 p.

Überall, H. & W. Madigosky (1998) Interface Waves on a Compliant Coating Bounded by a Fluid Flow and Their Excitation by Acoustic Resonance, *Proc. Int'l. Symp. Seawater Drag Reduction*, pp. 219–21

Van Manen, J. D. & P. Van Oossanen (1988) Resistance. *Principles of Naval Architecture*, E. V. Lewis, Ed., SNAME, Jersey City, NJ, Vol II, p 1–125.

Wang, J., Lan, S. & Chen, G. (2000) Experimental Study on the Turbulent Boundary Layer Flow Over Riblets Surface. *Fluid Dynamics Research*, **27**:217–29.

Warholic, M. D., H. Massah & T. J. Hanratty (1999) Influence of Drag Reducing Polymers on Turbulence: Effects of Reynolds Number, Concentration and Mixing. *Experiments in Fluids*, **27**:461–72.

White, F. M. (1991) *Viscous Fluid Flow*, University of Rhode Island, McGraw-Hill,

Wolfgang S. W., M. A. Tolkoff, A. H. Techet, D. S. Barret, M. S. Triantafyllou, D. K. P. Yue, F. S. Hover, M. J. Grosenbaugh & W. R. McGillis (1998) Drag Reduction and Turbulence Control in Swimming Fish-Like Bodies, *Proc. Int'l. Symp. Seawater Drag Reduction*, pp. 463–69

Wyatt, D. C. & P. A. Chang. (1994) Development and Assessment of a Total Resistance Optimized Bow for the AE-36. Marine Technology, 31(2):149–60

Yeh, H. Y. H. (1965) Series 64 – Resistance Experiments on High-Speed Displacement Forms, *Marine Technology* 2-3

Appendix A

Appendix A: FDR Assessment Table (Detail)

FDR Type & Author(s)	% drag reduction	Size of test platform	Tested body geometry	Test Re	Test freestream flow speed	Test body roughness	Test pressure gradient	Unsteady flow or pressure	Test fluid type (freshwater or otherwise)	Application	Notes
Riblets											
Hoyt, J. W., 1998	< 8%		flat plate, pipe, torpedo								
Mochizuki, S., and Osaka, H., 1998	10% @ Reθ = 1500	0.5 x 4 m	flat plate	600 < Reθ < 5000		smooth	zero	steady	air		
Anderson, G. W., Rohr, J. J., and Stanley, S. D., 1993	< 7%	0.025 x 3.7 m	pipe	2e5 < ReD < 6e5					fresh water	riblet appliqué	
Compliant walls											
Carpenter, P., 1998	< 7%										
Biofouling											
Schultz, M., and Swain, G., 1998	-33% to -187% Cf	0.6 x 2.1 m	flat plate	5500 < Reθ < 19100	1.2-4.0 m/s	bio-fouled	zero	steady	sea water		Cf scaling
Polymers											
Hoyt, J. W., 1998	< 60%	1m	flat plate	ReL < 10e7						angled nozzels	
Kulik, V. M., 1998	< 85%	0.002 x 4 m	pipe	ReD < 10e6	40 m/s	smooth			fresh water	angled nozzels	
Philips, R. B., Castano, J. M., and Stace, J., 1998	< 65%	0.35 x 2.73 m	flat plate		7.6 m/s	smooth			salt water	poly: nozzel, bubble: porous plate	Synergy w/ microbubbles
Oliver, D. R., and Bakhtiyarov, S. I., 1983	< 40%	0.006 x 3.1 m	pipe	ReL = 1.2e4					fresh water		
Ptasinski, P. K., Nieuwstadt, F. T. M., Van Den Brule, B. H. A. A., and Hulsen, M. A., 2001	< 70%	0.04 x 34 m	pipe	ReL = 1e4					fresh water		
Metzner, A., 1977	< 94%	0.024 to 0.070 m dia. pipe	pipe	4e4 < ReD < 2e5						fibers suspended in polymer solution	fiber/polymer synergy
High-Viscosity Fluid											
Kato, H., Fujii, Y., Yamaguchi, H., Miyanaga, M., 1993	< 60%	0.05 x 0.27 m	flat plate		5.9-10.2 m/s	smooth	inadvertant positive and random effects		fresh water	angled nozzels	Fluid: high concentration sugar-water

Appendix A: FDR Assessment Table (Detail)

FDR Type & Author(s)	% drag reduction	Size of test platform	Tested body geometry	Test Re	Test freestream flow speed	Test body roughness	Test pressure gradient	Unsteady flow or pressure	Test fluid type (freshwater or otherwise)	Application	Notes
Surfactants											
Kawaguchi, Y., Takehiko, S., Ziping, F., and Li P., 2002	< 80%										
Kawaguchi, Y., Takehiko, S., Ziping, F., and Li P., 2002	< 60%	0.04 x 5.0 m	flat plate	ReL = 5e4							
Myska, J., Zakin, J. L., and Chara, Z., 1996	< 30%	0.04 x 2.0 m	pipe		0.6-3.2 m/s	smooth			fresh water	recirculated fluid	
Microbubbles											
Guin, M. M., Kato, H., and Takahashi, Y., 1998	< 60%	0.1 x 0.7 m	flat plat	50e3 < ReL < 90e3	4.6-16.7 m/s	smooth	zero		fresh water	sintered plastic porous plate	
Latorre R., and Babenko, V., 1998	70-90%	1m	submersible		0.33-2.0 m/s					electrolysis	Electrolysis, ref 1
Latorre R., and Babenko, V., 1998	20-100%		flat plate		4.36-10.9 m/s					porous plate	Bottom screen, ref 3
Latorre R., and Babenko, V., 1998	65-100%	0.1-3.0 m	flat plate		5-7 m/s					porous plate	Top screen, ref 4
Latorre R., and Babenko, V., 1998	20-100%	0.6 x 0.6 m	flat plate		8 m/s					angled nozzels	ref 5
Bogdevich, V. G., Maltzev, L. I., and Maluga, A. G., 1998	< 30%	0.35 x 0.91 m	flat plate		3 m/s	smooth				porous plate	
Bogdevich, V. G., Maltzev, L. I., and Maluga, A. G., 1998	< 65%	0.18 x 1.75 m	axisymmetrical model		3 m/s	smooth				porous plate	
Kodama, Y., 1998	< 35%	0.1 x 3.0 m	flat plate		5-10 m/s	smooth			fresh water	porous plate	
Philips, R. B., Castano, J. M., and Stace, J., 1998	< 65%	0.35 x 2.73 m	flat plate		7.6 m/s	smooth			salt water	poly: nozzel, bubble: porous plate	Synergy w/ polymers
Madavan, N. K., Deutsch, S., and Merkle, C. L., 1985	< 80%	0.1 x 0.25 m	flat plate		4.2-17.4 m/s		zero		fresh water	sintered metal porous plate	

Appendix A: FDR Assessment Table (Detail)

FDR Type & Author(s)	% drag reduction	Size of test platform	Tested body geometry	Test Re	Test freestream flow speed	Test body roughness	Test pressure gradient	Unsteady flow or pressure	Test fluid type (freshwater or otherwise)	Application	Notes
Microbubbles (con't)											
Kato, H., Miyanaga, M., Haramoto, Y., Guin, M. M., 1994	< 80%	0.05 x 0.27 m	flat plate		8-10 m/s	smooth	inadvertant positive and random effects		fresh water	bubbly water through angled nozzels	*Energy balance estimate!, p. 192
Madavan, N. K., Deutsch, S., and Merkle, C. L., 1984	60-80%	0.1 x 0.25 m	flat plate		4.2-17.4 m/s		zero		fresh water	sintered metal porous plate	effects of plate orientation
Merkle, C. L., and Deutsch, S., 1992	< 40%	0.04 x 0.05 m	rectangular pipe	ReD < 2.2e5	8.3 m/s		zero		fresh water	sintered metal porous plate	*Energy balance estimate!, pp. 124-125
Merkle, C. L., and Deutsch, S., 1992	< 85%	0.24 x 0.05 m	flat plate	1.5e6 < ReL < 3.7e6	4.4-10.9 m/s		zero		fresh water	porous plate	
Merkle, C. L., and Deutsch, S., 1992	< 80%	0.18 x ? m	flat plate		2-6 m/s		zero		fresh water	porous plate	
Merkle, C. L., and Deutsch, S., 1992	< 80%	0.1 x 0.43 m	flat plate	2.8e6 < ReL < 1.0e7	4.5-17 m/s				fresh water	porous plate	
Merkle, C. L., and Deutsch, S., 1992	< 40%	0.09 x 0.63 m	axisymmetrical model	2.8e6 < ReL < 1.0e7	4.5-17 m/s				fresh water	porous plate	
Merkle, C. L., and Deutsch, S., 1992	?	0.31 x 1.1 m	flat plate	2.8e6 < ReL < 1.0e7	4.5-17 m/s				fresh water	porous plate	
Maltzev, L. I., 1995	< 85%		flat plate	ReL < 1.8e6	6 m/s				fresh water	air through angled nozzel	
Maltzev, L. I., 1995	< 50%	0.07 x 0.7 m	axisymmetrical model	ReL < 7e6	10 m/s				fresh water	air through angled nozzel	
Maltzev, L. I., 1995	< 50%	0.1 x 1.5 m	axisymmetrical model	ReL < 2.3e7	15 m/s				fresh water	bubbly water through angled nozzel	
Fibers											
Metzner, A., 1977	< 22%	0.024 to 0.070 m dia. pipe	pipe	ReD = 5e4, 1e5						fibers suspended in solution	
Metzner, A., 1977	< 94%	0.024 to 0.070 m dia. pipe	pipe	4e4 < ReD < 2e5						fibers suspended in polymer solution	fiber/polymer synergy

Appendix A: FDR Assessment Table (Detail)

FDR Type & Author(s)	% drag reduction	Size of test platform	Tested body geometry	Test Re	Test freestream flow speed	Test body roughness	Test pressure gradient	Unsteady flow or pressure	Test fluid type (freshwater or otherwise)	Application	Notes
Ventilation											
Fukuda, K., Tokunaga, J., Nobunaga, T., Nakatani, T., Iwasaki, T., and Kunitake, Y., 2000	< 60%	0.4 x 1.85 m	flat plate	4e6 < ReL < 17e6	2-10 m/s	smooth			fresh water	separate nozzel	Synergy w/ repellent coating
Fukuda, K., Tokunaga, J., Nobunaga, T., Nakatani, T., Iwasaki, T., and Kunitake, Y., 2000	< 85%	0.15 x 0.3 x 12.0 m	ship model		1-6 m/s	smooth	various	free surface effects	fresh water	angled nozzel	Synergy w/ repellent coating
Latorre R., 1997	< 12%	14.0 x 84.6 m	barge hull							nozzel & air pocket	+(2-3)% air blower power
Electrokinetics											
Fan, X., and Brown, G., 1998	< 5%	0.075 x 1.0 m	axisymmetric model		5.5 m/s	smooth (rust)			salt water		
O'Sullivan, P. L., and Biringen, S., 1998	-5% to + 5%		numerical model								
Du, Y., Crawford, C. H., and Karniadakis, G. E., 1998	< 5%		numerical model								
Wall Oscillation											
Choi, K. and Clayton, B., 1998	< 45%	0.5 x 0.5 m	flat plate	Reθ = 1190	2.5 m/s		zero		air		
Baron, A., and Quadrio, M., 1996	< 40%		flat plate	$Re_{u\tau} = 200$						DNS	
Blowing/Suction											
Choi, H., Moin, P., and Kim, J., 1994	< 25%		flat plate	ReD = 1800 and 3300						DNS	
Laminar body											
Wolfgang S. W., Tolkoff, M. A., Techet, A. H., Barret, D. S.,Triantafyllou, M. S., Yue, D. K. P., Hover, F. S., Grosenbaugh, M. J. & McGillis, W. R., 1998	< 70%	0.2 x 0.3 x 1.25 m	robot tuna fish	8.3e5 < ReL <9.6e5		smooth		unsteady	fresh water		

Appendix B

Appendix B: Brief Review of Numerical Methods

There are a number of computational and numerical analysis tools available to allow the hydrodynamicist to discern certain characteristics of fluid flow, either on or around a body, or flow far from a boundary. The computational tool utilized is frequently determined by the question one seeks to answer. The computational tools can be separated into six groups, each with its own strengths and shortcomings (Ferziger, 1996): correlations between fluid parameters and fluid behavior, integral equations, Reynolds averaged Navier-Stokes (RANS) equations, multi-point statistical models, large eddy simulation (LES) models, and direct numerical simulation (DNS) models.

One of the most fundamental and useful correlations is the known as the law of the wall, the basic analytical turbulent boundary layer scaling law. A significant body of experimental evidence supports this law. Very near the wall, the boundary layer is dominated by viscous shear. For $y^+ \leq 5$,

$$u^+ = y^+ \tag{B1}$$

where

$$u^+ = \frac{\bar{u}}{u_\tau} \tag{B2}$$

$$y^+ = \frac{y u_\tau}{\nu} \tag{B3}$$

$$u_\tau = \left(\frac{\tau_w}{\rho}\right)^{1/2} \quad \text{(sometimes referred to as the shear velocity)} \tag{B4}$$

Beyond this viscous sublayer is the overlap layer, located $5 \leq y^+ \leq \sim 300$ (possibly beyond), which can be described by

$$u^+ = \frac{1}{\kappa}\ln(y^+) + B \text{ in inner coordinates, or} \tag{B5}$$

$$U_\infty^+ - u^+ = \frac{1}{\kappa}\ln\left(\frac{y}{\delta}\right) + A \text{ in outer coordinates} \tag{B6}$$

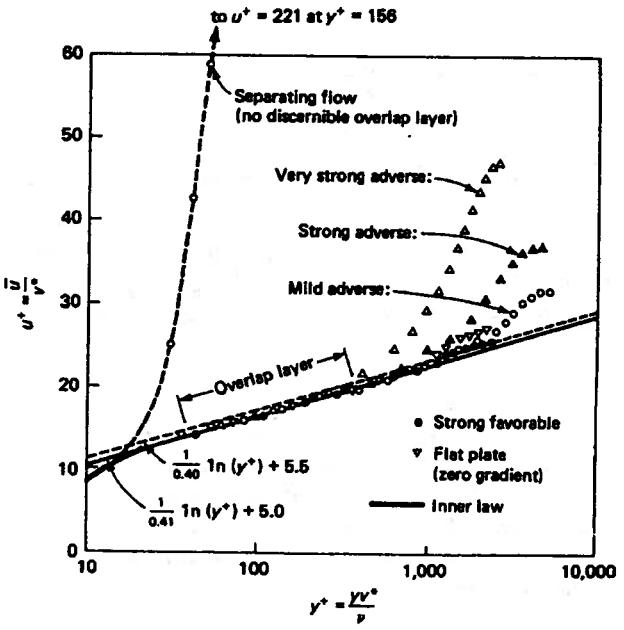

Figure B1: The Law of the Wall demonstrating the effect of pressure gradient (White, 1991)

The overlap layer is usually divided into two regions: the buffer layer, directly above the viscous sublayer, located $5 < y^+ \leq \sim 30$; and the logarithmic layer, located $\sim 30 < y^+ \leq \sim 300$. The values for κ, B and A are empirically derived, with commonly accepted values of $\kappa \approx 0.41$, and $B \approx 5.0$. The value of A is dependent upon the pressure gradient parameter, ξ, and other parameters as well, where

$$\xi = \frac{\delta}{\tau_w} \frac{dp_\infty}{dx} \tag{B7}$$

The value of A can very from 1.0 for a strongly favorable pressure gradient, to 2.5 for a zero pressure gradient, to 13 for a strongly adverse pressure gradient. Other equally effective formulas have been derived (White, 1991; DeGraaff and Eaton, 2000; Mathieu and Scott, 2000). Beyond $y^+ \approx 300$, the highly turbulent outer boundary layer exhibits a wake-like shape (a long, lazy "S") when viewed from the free stream.

The previous analysis assumes a perfectly smooth surface, over which the fluid flows. This is not likely to be the case for the ship hull plating. The David Taylor Model Basin conducted an analytical and experimental study of the effects of surface roughness on fluid flow (Granville, 1958). Equations for the law of the wall are modified with additional parameters to reflect the effects of increased surface roughness, where the non-dimensionalized surface roughness value $k^* = u_\tau k/\nu$, k is the length or size of the roughness.

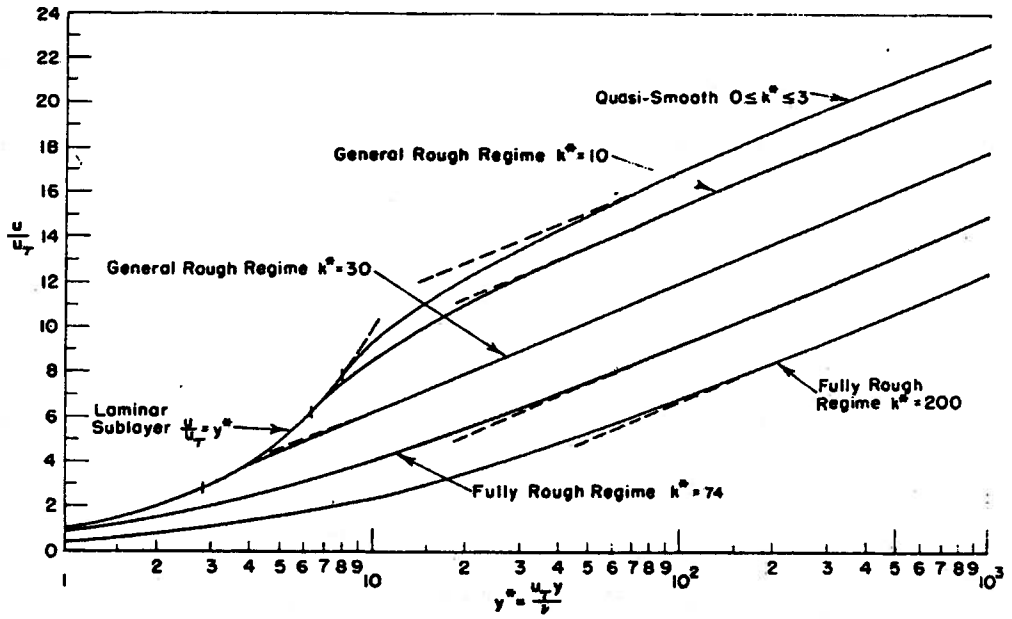

Figure B2: The Law of the Wall demonstrating the effect of added roughness (Granville, 1958)

Dimensional analysis correlations such as the law of the wall, friction factor or drag coefficient, with respect to Reynolds number, etc., are useful for comparing or describing the gross flow characteristics, or rough approximations, for simple geometries near the body boundary. However, in order to discern the fundamental physics of the complex flows around a hull or propulsion device in order to apply the most appropriate fluid drag reduction technology, we need to look at the flow data in a different way.

Integral equations such as the Blasius boundary layer solution or the Von Karman momentum integral equations are useful for estimating the boundary layer thickness over relatively simple geometries. The results gained can subsequently be used to estimate wall shear stress, and ultimately skin friction drag. These methods can also be useful for estimating the point of boundary layer separation, but aren't useful in estimating the resulting form drag due to that separation. Integral methods can be very useful for evaluating the gross behavior of the flow over the entire body, which can answer the ultimate question of how the body (ship) will behave due to the effect of the

fluid drag reduction technology. However, similar to the tools derived from dimensional analysis, we can use this method to get the level of detail necessary.

The Reynolds averaged Navier-Stokes (RANS) equations (sometimes referred to as single-point statistical equations) are obtained by writing every flow characteristic variable of the Navier-Stokes equations as an averaged value (averaged over time), and a fluctuating value:

$$\phi(x_i,t) = \overline{\phi}(x_i) + \phi'(x_i,t) \tag{B8}$$

where

$$\overline{\phi}(x_i) = \lim_{T\to\infty} \frac{1}{T} \int_0^T \phi(x_i,t) \cdot dt \tag{B9}$$

Averaging the flow characteristic over time is typical for a stationary process; a process in which the statistics of the variable are independent of time. The time averaging interval, T, must be large compared to the typical time scale of the fluctuations (Ferziger, 1996). The statistical characteristics of non-stationary processes (*e.g.* long term increase or decrease in velocity) should be determined by ensemble averaging, where the average value is determined by averaging over a large number, N, of data records:

$$\overline{\phi}(x_i) = \lim_{N\to\infty} \frac{1}{N} \sum_1^N \phi_n(x_i,t) \tag{B10}$$

However, to perform ensemble averaging properly, a large collection of identical experiments, performed under identical conditions, need to be performed. For many non-stationary processes that we are interested in studying, there are many non-controllable external variables that influence the fluid flow (*e.g.* stochastic seas around a complex hull form). Therefore, attempting to determine flow characteristics by ensemble averaging may not be appropriate or practical. Consequently, for a non-stationary process, the average value of a process characteristic is sometimes time averaged, choosing a appropriate time averaging interval. This interval must be significantly larger than the average turbulent fluctuation time interval, yet smaller than the long time interval over which the process characteristic changes. Choosing the proper time averaging interval for analyzing non-stationary processes can be an art as much as a science.

Decomposing the mean and fluctuating velocity and pressure terms produces the RANS equations:

$$\frac{\partial \overline{U}_i}{\partial t} + \overline{U}_i \frac{\partial \overline{U}_i}{\partial x_j} = -\frac{1}{\rho}\frac{\partial \overline{P}}{\partial x_i} + \nu \frac{\partial^2 \overline{U}_i}{\partial x_j \partial x_i} - \frac{\partial \overline{u_i' u_j'}}{\partial x_j} \tag{B11}$$

and

$$\frac{\partial \overline{U}_i}{\partial x_i} = 0 \tag{B12}$$

The Reynolds tensor, $-\overline{u_i' u_j'}$, represents the average momentum flux due to turbulence at a single point, and its value plays a role both in the creation and dissipation of turbulence. However, the RANS system of equations is not closed, requiring an empirically or analytically derived turbulence model to complete the equations. Various turbulence closure models have met with varying degrees of success, often depending on the type of flow, and the structure of the coordinate grid. Attempts to close the RANS equations through conservation relations (e.g. kinetic energy) are met with ever-higher order terms, for which empirical substitutions must be found. Some single-point and multi-point empirical substitutions appear to successfully generate analytical models that mirror the observed flow, but have limited supporting evidence for the empirical formula itself. A widely used empirical model for $-\overline{u_i' u_j'}$ is the eddy viscosity model, which treats the turbulence as an additional viscosity, where

$$-\overline{u_i'u'}_j = -\frac{1}{3}\overline{u_i'u_i'}\delta_{ij} + \nu_T\left(\frac{\partial \overline{U}_i}{\partial x_j} + \frac{\partial \overline{U}_j}{\partial x_i}\right) \tag{B13}$$

where $\nu_T = \nu_T(x_i,t)$ is the eddy-viscosity, representing the influence of turbulence on the mean flow. Additional closure methods can be reviewed in Ferziger (1996), and Mathieu and Scott (2000). The tensor terms are not only related to physical fluid properties, as the laminar shear term is, but are also related to local flow conditions such as velocity, geometry, surface roughness, and upstream history, making it difficult for empirical analysis alone to uncover the physics behind the observed behavior.

Solutions to the RANS equations can provide more fluid flow characteristics over complex bodies than the integral equations, such as fluid velocity, turbulence intensity, and pressure at any given point in the flow. It is at this level of sophistication that we begin to obtain the type of information that can be useful to the naval architect in order to improve a hull or propeller design.

Two-point or multi-point statistical models use the same concept of statistical averaging as the RANS equations, but correlate the velocity components at two, or more, distinct points. This method is rarely used except for homogenous turbulence analysis, and isn't of much use for analyzing flow over complex geometries. This technique is more frequently used for atmospheric analysis.

Large eddy simulation (LES) solves for the largest scale motions of the flow, while utilizing a turbulence model for the small scale motions. This method can be considered as a compromise between the RANS method, and DNS, providing more accuracy than RANS, and requiring much less computing power than DNS.

In order to reduce computing power, LES utilizes the concept of using a velocity field that contains only the large scale components of the total field (Ferziger, 1996). The large scale velocity field needs to be representative of the velocities between the large scale grid points. This is accomplished by filtering; it is a filtered set of conservation equations that is solved instead of the RANS equations. The large scale field (the one to be calculated), is an average of the complete field. The velocity filter is defined by

$$\overline{u}_i(x) = \int G(x,x') \cdot u_i(x') \cdot dx' \tag{B14}$$

where $G(x,x')$ is the filter kernel. Filter kernels that have been utilized include a Gaussian, a simple local average, and a cutoff (eliminating all Fourier coefficients belonging to wave numbers above the cutoff). Every filter has a length scale, Δ, associated with it, but this length scale does not necessarily correspond to the distance between data grid points.

Decomposing the filtered and fluctuating velocity and pressure terms produces equations very similar to the RANS equations [B11] and [B12], including an unresolved subgrid scale (SGS) Reynolds stress:

$$\tau_{ij}^s = -\rho\left(\overline{u_i u_j} - \overline{u}_i\overline{u}_j\right) \tag{B15}$$

As with the RANS Reynolds stress, the SGS Reynolds stress isn't really a stress, but rather the large scale momentum flux caused by the small, unresolved scales (Ferziger, 1996). Smagorinsky (1963) developed an eddy viscosity model for the SGS Reynolds stress that is commonly used

$$\tau_{ij}^s - \frac{1}{3}\tau_{kk}^s\delta_{ij} = \mu_t\left(\frac{\partial \overline{u}_i}{\partial x_j} + \frac{\partial \overline{u}_j}{\partial x_i}\right) = 2\mu_t\overline{S}_{ij} \tag{B16}$$

where μ_t is the eddy viscosity and $\overline{S_{ij}}$ is the strain rate of the large scale field:

$$\mu_t = C_s^2 \rho \Delta^2 \mid \bar{S} \mid \tag{B17}$$

$$\mid \bar{S} \mid = \left(\bar{S}_{ij} \bar{S}_{ij}\right)^{1/2} \tag{B18}$$

C_s is a turbulence model parameter, and is not constant. $C_s \approx 0.2$ for isotropic turbulence, but that is not the type of turbulence experienced near a boundary. One model for C_s is the van Driest damping model, which has been successfully used to reduce near-wall eddy viscosity in RANS analysis:

$$C_s = C_{s0}\left(1 - e^{-y^+/A^+}\right)^2 \tag{B19}$$

where y^+ is the distance from the wall in viscous wall units, and A^+ is a constant usually taken to be about 25.

Another problem near the wall is that the flow structure is very anisotropic due to alternating regions of low speed streaks and higher speed fluid, requiring an anisotropic grid, and an appropriate choice of length scale. It may be that the length scale in each coordinate direction, Δ_i, should be different. Ferziger (1996) raises the possibility that with the appropriate choice of grid and length scale, damping the near-wall turbulence as seen in [B19], may not be necessary.

DNS models solve the unsteady, three-dimensional Navier-Stokes equations directly without filtering, averaging, or using approximations, with the exception of those associated with discretization, which can be estimated and controlled. DNS has the ability to execute numerical experiments that are often either difficult, or impossible, in the laboratory, and yield detailed information down to the smallest scales, and has been used to good effect to confirm the formation and lift-up of the hairpin vortices near a surface, in turbulent flow, that was observed in laboratory experiments.

In order to capture all of the turbulent flows within a fluid domain, the domain must be large enough to enclose the largest turbulent structures, as well as be subdivided by a grid fine enough to permit kinetic energy dissipation (a viscous scale, called the Kolmogoroff scale). The extreme accuracy required makes the use of spectral methods popular for DNS and LES (essentially obtaining derivatives by Fourier series). However, these methods lend themselves only to certain types of equally spaced grids. Due to the sensitivity of the DNS analysis to initial and boundary conditions, they must be established to be as realistic as possible. The further the initial and boundary conditions are from actual, the longer the DNS may have to run (meaning more expense) in order to observe the fluid behavior under desired conditions.

The result of a DNS analysis returns velocities, pressure, and stresses at every point at every infinitesimal increment in time. While this information can be very useful for certain investigations, it is an unnecessarily expensive use of time and resources for design by the engineer or naval architect. LES or RANS methods, if well calibrated, will deliver all of the information necessary for design purposes. Ferziger (1996) concludes that, for the near future, DNS will be limited to a research tool. Examples of where DNS has been useful are:

- Understanding the mechanisms of turbulence production, energy transfer, and dissipation in turbulent flows
- Simulation of the production of aerodynamic noise
- Understanding the effects of compressibility on turbulence
- Understanding the interaction of combustion and turbulence
- Controlling and reducing drag on a solid surface